

1 **Title:**

2 Humanized nucleosomes reshape replication initiation and rDNA/nucleolar integrity in yeast.

3

4 **Authors:** Luciana Lazar-Stefanita<sup>1\*</sup>, Max A. B. Haase<sup>1,2</sup>, Jef D. Boeke<sup>1,3\*</sup>

5

6 Lead Contact: Jef D. Boeke, [jef.boeke@nyulangone.org](mailto:jef.boeke@nyulangone.org)

7

8 **Affiliations:**

9 <sup>1</sup>Institute for Systems Genetics and Department of Biochemistry and Molecular Pharmacology,  
10 NYU Langone Health, New York, NY 10016, USA

11 <sup>2</sup>Vilcek Institute of Graduate Biomedical Sciences at NYU School of Medicine, NY 10016, USA

12 <sup>3</sup>Department of Biomedical Engineering, NYU Tandon School of Engineering, Brooklyn, NY  
13 11201, USA

14 \*Correspondence: L.L.-S., [luciana.lazarstefanita@nyulangone.org](mailto:luciana.lazarstefanita@nyulangone.org), J.D.B.

15 [jef.boeke@nyulangone.org](mailto:jef.boeke@nyulangone.org)

16

17 **Highlights:**

18 Humanized nucleosomes wrap 10 additional nucleotides, shortening free linker length

19 Histone-humanized nucleosomes have increased occupancy for DNA

20 Humanized nucleosomes potentially decrease chromatin accessibility by blocking-out free linker  
21 DNA

22 Nucleosome humanization impedes DNA replication by affecting chromatin structure at origins

23 Humanized nucleosomes reversibly destabilize the ribosomal DNA array and leads to massive  
24 intrachromosomal rDNA locus expansion

25 Histone humanization disrupts rDNA silencing and leads to nucleolar fragmentation

26 **Summary**

27 Eukaryotic DNA wraps around histone octamers forming nucleosomes, which modulate genome  
28 function by defining chromatin environments with distinct accessibility. These well-conserved  
29 properties allowed “humanization” of the nucleosome core particle (NCP) in *Saccharomyces*  
30 *cerevisiae* at high fitness costs. Here we studied nucleosome-humanized yeast-genomes to  
31 understand how species-specific chromatin affects nuclear organization and function. We found  
32 a size increase in human-NCP, linked to shorter free linker DNA, supporting decreased  
33 chromatin accessibility. 3-D humanized-genome maps showed increased chromatin compaction  
34 and defective centromere clustering, correlated with high chromosomal aneuploidy rate. Site-  
35 specific chromatin alterations were associated with lack of initiation of early origins of replication  
36 and dysregulation of the ribosomal (rDNA and rRNA) metabolism. This latter led to nucleolar  
37 fragmentation and rDNA-array instability, through a non-coding RNA dependent mechanism,  
38 leading to its extraordinary, but entirely reversible, intra-chromosomal expansion. Overall, our  
39 results reveal species-specific properties of the NCP that define epigenome function across vast  
40 evolutionary distances.

41

42 **Keywords**

43 Nucleosome humanization, chromatin structure, genome instability, DNA replication, ribosomal  
44 DNA array, nucleolus.

45 **Introduction**

46 In eukaryotes DNA molecules are packed in the nucleus in a hierarchical folding structure. The  
47 first level of organization consists of ~1.7 superhelical turns of 147 bp DNA around an octamer  
48 of two copies each of the four histone proteins: H2A, H2B, H3 and H4 (reviewed in McGhee and  
49 Felsenfeld<sup>1, 2</sup>). Altogether they form the nucleosome core particle (NCP) that constitutes the  
50 basic structural unit of chromatin<sup>2,3</sup>, conserved throughout eukaryotes (reviewed in Kornberg  
51 and Lorch<sup>4</sup>, Malik and Henikoff<sup>5</sup>). Aside from the canonical core histones, the sequence-  
52 specified centromere of *Saccharomyces cerevisiae* (~120 bp AT-rich region) is organized into a  
53 specialized nucleosome containing Cse4, a centromere-specific variant of histone H3<sup>6–8</sup>. A  
54 single Cse4 nucleosome is thought to form the minimal unit of the point centromeric  
55 chromatin<sup>7,9</sup>, required for the recruitment of the kinetochore complex and proper chromosome  
56 segregation (reviewed in Cleveland et al.<sup>10</sup>). Genome-wide footprinting showed that the  
57 centromeric nucleosome contains a micrococcal nuclease-resistant unit of ~123–135 bp,  
58 significantly shorter than the canonical nucleosome<sup>11</sup>.

59

60 Nearly 80% of the yeast DNA is incorporated into stable nucleosomes<sup>12</sup>. The “chromatinization”  
61 process takes place primarily during S-phase and is coupled to the passage of the DNA  
62 replication fork<sup>13</sup>, when parental and de novo synthesized histones are deposited onto the two  
63 nascent DNA molecules<sup>14–17</sup>. During this process, histone chaperones and nucleosome  
64 remodelers closely interact with components of the replication machinery to deposit new and old  
65 histone octamers onto the newly replicated duplexes<sup>18</sup> (reviewed in Budhavarapu et al.<sup>19</sup>, Sauer  
66 et al.<sup>20</sup>). The DNA sequence interconnecting consecutive NCPs to form higher-order structures  
67 is called the linker<sup>4</sup>. Its length varies among cell types and organisms (e.g., ~20 bp long in *S.*  
68 *cerevisiae*<sup>21</sup>), and is thought to be inversely correlated with gene activity<sup>22–25</sup>. In addition,  
69 correctly stabilizing nucleosome positions on the DNA polymer - relative to *cis* regulatory  
70 elements (e.g., replication origins and transcription start sites) - is a critical component of  
71 genome function and regulation (reviewed in Rando and Chang<sup>26</sup>, Lai and Pugh<sup>27</sup>). Regions of  
72 the genome that are devoid of nucleosomes, referred to as nucleosome-free regions (NFRs),  
73 represent accessible parts of the chromatin where multiprotein complexes can assemble and  
74 regulate/perform key DNA-templated processes e.g., replication and transcription<sup>27</sup>. As these  
75 processes occur in the context of the surrounding chromatin environment, nucleosome  
76 occupancy and positioning can restrict access to particular DNA sequences and influence  
77 genome-wide initiation/firing of origins of replication<sup>28,29</sup> and transcription regulation (reviewed in  
78 Bai and Morozov<sup>30</sup>). Ergo post-translational modifications of nucleosomes, defining distinct local

79 chromatin environments, also affect these processes (reviewed in Bowman and Poirier<sup>31,32</sup>).  
80 Furthermore, it has been proposed that the epigenetic information is maintained during  
81 transcription and replication<sup>33</sup>, and can even be transmitted through generations (reviewed in  
82 Kaufman and Rando<sup>34</sup>, Campos et al.<sup>35</sup>). On the other hand, yeast nucleosomes that lack  
83 certain post-translational modifications (e.g., acetylation) are associated with silenced  
84 chromatin. The hypoacetylated nucleosomes promote a compact chromatin structure (or  
85 heterochromatin) and makes DNA inaccessible to processes such as transcription and  
86 replication initiation (reviewed in Gartenberg and Smith<sup>36</sup>). The Sir2 (Silent information regulator  
87 2) protein is a conserved NAD<sup>+</sup>-dependent deacetylase that removes key acetyl groups from  
88 histone H3 (H3K9 and H3K14) and H4 (H4K16)<sup>37,38</sup>. This type of epigenetic silencing occurs at  
89 diverse genomic sites including the silent *HM*-mating type loci, telomeres and the ribosomal  
90 DNA (rDNA) tandem array. Hypoacetylated H3 and H4 histones<sup>39</sup> have been linked with  
91 heterochromatin formation by establishing direct interactions with components of the silencing  
92 complex (Sir3/4) and nucleosomes<sup>40-42</sup>. These interactions not only participate in telomere and  
93 *HM* loci silencing, but also in their nuclear envelope positioning<sup>43</sup>. Finally, only Sir2 deacetylase  
94 activity is required for rDNA silencing whereas Sir3/4 are dispensable<sup>44,45</sup>.  
95

96 Despite the vast evolutionary distance between yeast and human, large-scale systematic  
97 studies have found that several hundred yeast genes can be individually replaced with their  
98 human orthologs and sustain yeast growth (3%)<sup>46,47</sup> (reviewed in Dunham and Flower<sup>48</sup>). Multi-  
99 gene interspecies swaps have also been reported<sup>49</sup>, exemplified by the humanization of the  
100 entire NCP (H2A, H2B, H3 and H4) of *Saccharomyces cerevisiae* (Truong and Boeke<sup>50</sup>).  
101 Although yeast and human histones are highly conserved (68% - 92% identity), isolation of  
102 NCP-humanized yeasts required acquiring genetic mutations to survive and they display  
103 dramatic phenotypic defects associated with a global RNA reduction. These findings presented  
104 the opportunity to examine the effects of human histones in yeast to provide valuable insights  
105 into the mechanisms that govern chromatin-related processes in distantly related organisms.  
106 Here we used yeast strains that rely on human histones for packaging their DNA molecules, to  
107 address how these species-specific units of chromatin structure alter yeast genome  
108 organization - from nucleosome fibers up to the 3D structure of chromosomes - and how these  
109 structural changes reflect upon biological processes (e.g., DNA replication, gene silencing and  
110 genome stability).

111

## 112 **Results**

113 To ascribe our findings to the type of histone used for DNA packaging (yeast vs. human), we  
114 compared results obtained from humanized strains carrying distinct “humanization-suppressing”  
115 mutations. This terminology was coined to indicate a specific subset of genetic mutations  
116 required for histone-humanized yeasts to survive and propagate<sup>50</sup>. Notably, some of these  
117 mutations were found to have distinct effects on genome stability, leading to isolation of two  
118 classes of humanized strains with distinct levels of aneuploidy. Here we focused on two such  
119 humanized yeast strains carrying each a single point mutation, in either *DAD1* (strain: yDT180,  
120 *dad1*-E50D) or *SCC4* (strain: yDT92, *scc4*-D65Y) genes, which display either normal or  
121 abnormal ploidy, respectively. These were isolated by Truong in 2017, and the mechanism of  
122 ploidy stabilization was addressed by Haase et al.<sup>51</sup> who documented that the mutation in *dad1*-  
123 E50D (component of the outer kinetochore DASH/Dam1 complex) stabilized ploidy of the  
124 histone-humanized yeasts by weakening the interaction between the outer kinetochore and the  
125 microtubules.

126

127 *Visualization of histone-humanized chromatin fibers in yeast.*  
128 Previously reported nucleosome occupancy maps have shown a high degree of structural  
129 conservation of histone-humanized chromatin fibers in yeast<sup>50,51</sup>, with notable exceptions  
130 described later in this manuscript. Even if nucleosome positioning appears to be well conserved  
131 overall, the details of the wrapping of yeast DNA on the human NCP remain unknown. To  
132 address this question, we used transmission electron microscopy (TEM) to directly image  
133 chromatin fibers extracted from yeast cells harboring either human or native yeast histones.  
134 Representative images in [Figure 1A](#) show the expected “beads-on-a-string” array arrangement  
135 of the nucleosomes in the wild-type, *Sc* (*Saccharomyces cerevisiae*), and in the histone-  
136 humanized, *Hs* (*Homo sapiens*), cells. The schematic in [Figure 1B](#) shows an example of an  
137 NCP used as a benchmark to calculate mononucleosome surface area. The latter was  
138 measured using chromatin images acquired at various resolutions (representative images are  
139 shown in [Figure S1](#) and [S2](#)) accounting for approximately 500 nucleosomes for each *Sc* and *Hs*  
140 strain ([Table S1](#)). Bee swarm plots in [Figure 1C](#) point to a small but significant increase in the  
141 surface of the mononucleosome in both histone-humanized strains (*Hs*: yDT92 and yDT180),  
142 relative to the WT (*Sc*: BY4742) yeast strain. This change corresponds to a ~5% increase in the  
143 circumference of the NCP (~1.8 nm) and suggests that more DNA in the nucleosome repeat  
144 length is wrapped/protected by the histone-humanized octamer compared to the native yeast  
145 one. Moreover, this result is quantitatively supported by an orthogonal method that directly  
146 measured DNA fragment size (using capillary electrophoresis) from MNase digested chromatin

147 and showed that the *Hs*-NCP protects ~10 bp more DNA than the *Sc*-NCP ([Figure 1D](#) data from  
148 Haase et al., co-submission). Importantly, this result excludes the possibility of imaging and  
149 analyzing semi-complete NCPs from yeast due to the lower intrinsic stability of the histone  
150 octamer in yeast compared to other metazoans<sup>52,53</sup> (reviewed in McGinty and Tan<sup>54</sup>). Since we  
151 did not detect any change in nucleosome positioning nor in the repeat length itself, it suggests  
152 that the extra 10 bp of protected sequence corresponds to a reduction in free linker DNA length  
153 in yeast. This finding provides *in vivo* reinforcement to the idea that human histone octamers  
154 associate more stably with DNA than the yeast ones and nucleosome packaging in higher-order  
155 chromatin structures is fundamentally different between these two species<sup>52,55</sup>. Finally, these  
156 results provide a structural underpinning for the general decrease in chromatin accessibility in  
157 the humanized yeast and provides a plausible explanation for their global downregulation of  
158 RNA (previously reported in Truong and Boeke<sup>50</sup>, Haase et al.<sup>51</sup>), presumably reflecting reduced  
159 access of RNA polymerases and/or transcription factors to DNA.

160

161 *3-Dimensional organization of the histone-humanized yeast genome.*

162 Next, we investigated if the nanoscale effects of histone humanization are echoed at longer  
163 genomic distances, affecting the overall spatial organization of chromosomes. Genome-wide  
164 proximity maps of the *Hs* and *Sc* yeast strains were generated using the chromatin  
165 conformation capture approach, Hi-C<sup>56</sup>. At first glance, the 2D (2-Dimensional)  
166 interaction/contact frequency maps of two representative chromosomes (chr I/V and chr V) in  
167 [Figure 2A](#) show that the typical organization of *S. cerevisiae*'s genome is preserved overall in  
168 both histone-humanized suppressor mutants (*Hs dad1-E50D* and *Hs scc4-D65Y*). The so-called  
169 Rabl-like organization<sup>57</sup> of yeast chromosomes is characterized by the spatial clustering of all  
170 peri-centromeric regions (indicated with black arrowheads in [Figure 2A](#)) and their relative  
171 insulation from the chromosomal arm sequences ([Figure 3C, upper schematic](#))<sup>58</sup>. Further  
172 analysis of intra-chromosomal contacts, that computes the decay in contact probability (*p*) as a  
173 function of the genomic distance (*s*), showed a small but reproducible increase of contacts at  
174 mid-range (~20-50 kb) distances in the *Hs* chromosomes relative to *Sc* ([Figure 2B](#)). In addition,  
175 the contact variation maps in [Figure 2C](#) not only confirmed an increase in mid-range intra-  
176 chromosomal contacts in the *Hs* strains, as shown by the red signal running parallel to the  
177 proximal diagonal, but they also revealed local contact variations surrounding the peri-  
178 centromeres. Here, the black arrowheads point to peri-centromeric positions which appear to  
179 favor interactions with the distal chromosomal arms, both in *cis* (within the same chromosome)  
180 and in *trans* (on different chromosomes), in the *Hs* relative to *Sc* maps. These stand out as red

181 contact stripes on the comparison maps and support the hypothesis that the centromeres are  
182 de-clustered in the *Hs* strains relative to the *Sc* strain. To test this hypothesis, we used the  
183 normalized *Hs* and *Sc* contact maps (expanded versions of the insets shown in [Figure 2A](#)) to  
184 quantify the frequency of contacts that each peri-centromeric region (50 kb sequence centered  
185 on a given centromere) makes with the remaining 15 peri-centromeres, where higher contact  
186 values correspond to robust centromere clustering. The left plot in [Figure 3A](#) reveals a  
187 significant reduction to the inter-centromere contacts in *Hs* compared to *Sc* of approximately  
188 30%. Notably this result was reproduced in both *Hs dad1-E50D* and *Hs scc4-D65Y* yeasts,  
189 suggesting that centromere de-clustering occurs regardless of the humanization-suppressor  
190 mutations in the histone-humanized strains ([Figure 3B](#), average 3-Dimensional representations  
191 of the Hi-C maps with a viewpoint on the centromeres in yellow). Based on DNA content  
192 analysis and chromosome coverage plots ([Figure S3A-B](#)), we confirmed that a specific subset  
193 of chromosomes tended to be aneuploid in *Hs scc4-D65Y*, whereas the genome of *Hs dad1-*  
194 *E50D* maintains normal ploidy (as previously reported in Truong and Boeke<sup>50</sup> and Haase et  
195 al.<sup>51</sup>). Given that centromeres are the key elements responsible for chromosome stability during  
196 cell division, we reasoned that peri-centromeres of aneuploid chromosomes may fail to achieve  
197 this function due to a further aggravated defect in their clustering. To explore this hypothesis, we  
198 first computed the inter-chromosome contact variations for both *Hs* strains with normal and  
199 aneuploid chromosomes (ratio of the normalized Hi-C maps: humanized vs. WT yeast, [Figure](#)  
200 [S3C](#)), which we used as a ploidy-correction to the inter-centromere contact variation between  
201 humanized and WT strains. The plot on the right in [Figure 3A](#) shows a further reduction (up to  
202 ~45%) in centromere clustering exclusive to the aneuploid (amber) chromosomes in *Hs scc4-*  
203 *D65Y* relative to the euploid (gray) chromosomes. Overall, our results show that humanization  
204 of the canonical histones in yeast destabilizes the structure of the peri-centromeric chromatin  
205 and leads to centromere de-clustering ([Figure 3C, lower schematic](#)). This provides structural  
206 support explaining the frequent chromosomal aneuploidies observed post-humanization.  
207

208 *Histone humanization delays activation timing of DNA replication origins.*  
209 Given the inseparable relationship between genome structure and function, we then asked  
210 whether structural changes introduced by humanized nucleosomes would affect specific  
211 biological processes. Our previous work has shown that the humanized yeasts have low  
212 fitness<sup>50</sup>, suffering from a prolonged cell cycle (~3-fold longer). One potential explanation for the  
213 cell cycle delay might be a defect in DNA replication initiation of histone-humanized

214 chromosomes, since recognition of replication origins might be blocked by the increased  
215 nucleosome stability/binding.

216 In *S. cerevisiae*, DNA replication start sites or origins (named Autonomously Replicating  
217 Sequences<sup>59</sup>) are marked by a degenerate T-rich motif, named ARS consensus sequence  
218 (ACS)<sup>60,61</sup> to which the heterohexameric origin recognition complex (ORC) binds<sup>62–64</sup>. During G1,  
219 ORC recruits the Mcm2–7 helicase to initiation sites (reviewed in Bell and Kaguni<sup>65</sup>), leading to  
220 the formation of the pre-replicative complex (pre-RC) that marks origin activation in S-phase  
221 (reviewed in Remus and Diffley<sup>66</sup>). Notably, among the >12000 high-quality ACS motifs, less  
222 than 300 of these function as origins of replication<sup>67</sup>, and only ~120 appear to fire early in S-  
223 phase, independent of the checkpoint activation induced by dNTPs pool depletion<sup>68</sup>. Although  
224 the precise mechanism underlying origin selection and their single-cell temporal heterogeneity  
225 (deterministic vs. probabilistic) remains a matter of debate, their activation is thought to be  
226 modulated locally - by epigenetic modifications of the chromatin (i.e., nucleosome positioning  
227 can restrict access to the ACS<sup>69</sup> and inhibit pre-RC assembly<sup>70</sup>) - and spatially in the context of  
228 the chromosome (i.e., proximity to a functional centromere<sup>71,72</sup>).

229 Here we used a well described method to map early firing ARS regions genome-wide in yeast  
230 cell populations<sup>68,72,73</sup>. Three independent isolates of each *Hs* and *Sc* strain were synchronized  
231 in G1 using a-Factor and released synchronously in S-phase in the presence of hydroxyurea  
232 (HU), that blocks DNA elongation and causes an early S-phase arrest through dNTP starvation  
233 (Figure S4A). Prior to genome-wide sequencing, the quality of G1 and S synchronizations were  
234 evaluated by measuring DNA content using flow cytometry (Figure S4B). Mapping of the early  
235 firing ARSs was done by computing chromosome sequence coverages in early-S normalized to  
236 G1 (unreplicated control) and plotted along the reference genome at 1 kb resolution. We  
237 observed that the prominent signal corresponding to early-firing origins (indicated by black  
238 arrowheads in Figure 4A) was severely compromised and often entirely lost in *Hs* (orange plot)  
239 compared to *Sc* (blue plot). This defective firing trend was particularly obvious on the longer  
240 chromosome arms (Figure S5). Note that the reduced firing intensity of the early-S regions in  
241 the *Hs* isolates is unlikely a result of incomplete synchronization, as we accounted for their  
242 extended cell cycle and corrected with accordingly prolonged incubations (Figure S4A). The  
243 firing defect was observed genome-wide (Figure S5 and Figure 4B, ratio of origin timing in *Hs*  
244 vs. *Sc*), independent of chromosome size and ARS location (i.e., distance from the early  
245 replicating centromere). Previous high-throughput nucleosome-positioning assays have shown  
246 that well-positioned nucleosomes flanking ARS consensus sequences are conserved functional  
247 features of replication origins<sup>29,74</sup> and are maintained by ORC binding<sup>28</sup>. We observed that the

248 positioning of the human nucleosomes forms the typical nucleosome-depleted region (NDR,  
249 centered on the ARS consensus); however, it is accompanied by unexpectedly higher  
250 nucleosome occupancy in the NDR-adjacent regions in both histone-humanized lineages  
251 (Figure 4C, MNase-seq profiles showing nucleosome profiles at ARSs). These results suggest  
252 that the innate increased stability of human nucleosomes<sup>52,53</sup> in yeast may have a powerful  
253 repressive effect that impinges not only the transcriptional program (shown by Truong and  
254 Boeke<sup>50</sup>), but also on origin firing during DNA replication. Collectively, these findings provide a  
255 mechanism to explain the previously reported cell cycle defect in the histone-humanized strains,  
256 imputed to a slow S-phase progression.

257

258 *Histone humanization causes instability of the ribosomal DNA array.*

259 Intriguingly, while analyzing the deep-sequencing data (Hi-C libraries and profiles of replication  
260 timing, above), we observed a substantial enrichment in multi-mapping reads in the histone-  
261 humanized yeast (from ~15% in *Sc* to ~35% in *Hs* strains). Closer examination of the multi-  
262 mapped reads, using the built-in commands in SAMtools<sup>75</sup> to sort and index the alignments,  
263 revealed that the vast majority of these originated from chromosome XII. In *S. cerevisiae*,  
264 chromosome XII harbors the highly repeated ribosomal DNA locus (rDNA; ~150-200 copies of  
265 rRNA genes)<sup>76</sup>, accounting for ~10-17% (~1.5 Mb) of the entire yeast genome (reviewed in  
266 Kobayashi and Sasaki<sup>77</sup>). Given its repetitive nature and the high demand for ribosomal RNA  
267 transcripts<sup>78</sup>, the rDNA locus is arguably the most unstable genomic structure (reviewed in  
268 Salim and Gerton<sup>79</sup>). Recombination events between rDNA repeats can lead not only to  
269 variability in the size of the locus (loci)<sup>80</sup> (reviewed in Kobayashi<sup>81</sup>), but also to the formation of  
270 extra-chromosomal rDNA circles (ERCs) thought to occur predominantly during replicative  
271 aging<sup>82,83</sup>. We therefore hypothesized that histone humanization may lead to rDNA instability  
272 and copy number amplification of the rRNA genes. To test whether rDNA amplification is extra-  
273 or intra-chromosomal, we performed a Pulsed-Field Gel Electrophoresis-Southern blot assay  
274 and found an extraordinary increase to the size of chromosome XII (expected size ~2.5 Mb in  
275 *Sc*) linked to the internal expansion of the rDNA locus (Figure 5A, BamHI digested  
276 chromosomes used to exclusively resolve the rDNA locus). The size of the rDNA expansion in  
277 the euploid *Hs dad1-E50D* clones exceeds the maximum resolution potential of the PFGE (5-6  
278 Mb) but forms a band, whereas, in the aneuploid *Hs scc4-D65Y* lineage the clones display a  
279 smaller smear-like migration of the rDNA that is likely a reflection of a population of rDNAs of  
280 different sizes on the aneuploid chromosome XII (Figure S6A). Intra-chromosomal expansion of  
281 the rDNA is also supported by the Hi-C maps (Figure S6B, insets of ratio maps between *Sc* and

282 *Hs* genomes showing *cis* and *trans* contact variations between chromosomes *XII* and *XIII*) and  
283 the corresponding 3D average representations of chromosomes (Figure 5B), in which the  
284 expansion of the locus causes the distal part of chromosome *XII/R* arm to be insulated from the  
285 remaining genome. Finally, we did not detect accumulation of ERCs in any of the *Hs* yeast  
286 strains compared to *Sc* (Figure S7, exonuclease treatment shows only the band of 2-micron  
287 plasmid), reinforcing the evidence of intra-chromosomal amplification of the rDNA array.  
288 To better understand the kinetics of the rDNA expansion following nucleosome humanization,  
289 we estimated the size of the locus in the euploid *Hs dad1-E50D* by computing the ratio between  
290 reads mapped to rDNA and the remainder of chromosome *XII* ("n" = number of independent  
291 genome-wide sequencing datasets, Table S2). We found that the expansion occurs very early  
292 on during histone humanization ("non-evolved" indicates genomic libraries prepared  
293 immediately after transforming the *Hs* histone plasmid and shuffling-out the *Sc* histones) and it  
294 reaches a maximum of 5-6 Mb (accounting for ~600 repeats) after passaging them for ~100  
295 generations (Figure 5C, *Hs* plots). Moreover, after "re-yeastification" – by re-introducing the *Sc*  
296 histones in the already histone-humanized strains – the physiological size of the rDNA locus  
297 was entirely rescued (Figure 5C, *Hs* + *Sc* plots). Therefore, we concluded that the expansion of  
298 the rDNA locus is a reversible adaptation that is entirely dependent on human histones. Next,  
299 we wanted to learn what epigenetic-dependent mechanism(s) allows for this switch in rDNA  
300 stability.

301

302 *Histone humanization causes rRNA metabolic dysregulation and disrupts nucleolar structure.*  
303 Each ribosomal DNA repeat unit (9.1 kb) not only encodes for the four ribosomal RNA genes  
304 (25S, 18S, 5.8S and 5S), but also contains two non-transcribed intergenic spacers (*NTS1* and  
305 *NTS2*) (reviewed in Nomura et al.<sup>84</sup>) thought to be involved in the metabolic regulation of rDNA  
306 array size<sup>85-87</sup> (reviewed in Kobayashi<sup>81</sup>) (Figure 6A). The amplification of this locus relies on a  
307 repeat-mediated homologous recombination mechanism that requires: (1) binding of Fob1  
308 protein to the rDNA replication fork block (*RFB*) site<sup>85,86,88,89</sup> and/or (2) lack of transcriptional  
309 silencing (mediated by SIR and cohesin complexes) of the NTS sequences<sup>87,90,91</sup>. We reasoned  
310 that changes in chromatin occupancy at the rDNA locus in the *Hs* histone strains could hint  
311 towards a potential mechanism responsible for the amplification of the array. MNase-  
312 sequencing profiles showed that the *Hs* nucleosome occupancies at the rDNA locus remained  
313 unexpectedly similar between the *RDN37* and the NTS regions compared to the *Sc* yeast  
314 (where NTS silencing allows for higher nucleosome occupancy) (Figure S8A), suggesting  
315 functional misregulation. Notably we detected increased occupancy at the ribosomal origin of

316 replication (*rARS*) in *NTS2* and at the RFB-Fob1 site in *NTS1* in the *Hs* histone strains vs. the  
317 *Sc* (Figure S8A). To validate whether RFB-Fob1 is responsible for the locus instability<sup>86</sup> in *Hs*  
318 histone yeasts, we deleted *FOB1* in *Sc* strain and found that after histone humanization, rDNA  
319 arrays invariably expanded (Figure S8B). We thus conclude that rDNA amplification in the  
320 histone-humanized yeasts does not rely on a replication-based mechanism, in agreement with  
321 the absence of ERC (as previously shown in Figure S7).

322 Notably, the MNase profiles in *Hs* histone strains showed a region of nucleosome depletion  
323 mapping to the rDNA bidirectional noncoding RNA polymerase II promoter (E-pro) (Figure S8A),  
324 we thus wondered whether rRNA and/or ncRNA (at the NTSs) transcripts are dysregulated at  
325 this locus. Triplicates of total RNA extractions from similar number of cells followed by gel  
326 quantifications showed that the rRNA polymerase I transcripts (25S and 18S) were ~2.5-fold  
327 reduced in the *Hs* strains (Figure 6B and S9B). This result suggests that histone-humanized  
328 cells contain less ribosomes, in line with their substantially reduced rRNA levels. In addition to  
329 the rRNA levels, we further investigated the transcriptional activity at the E-pro by measuring the  
330 levels of NTS transcripts using RT-qPCR and RNA-seq. We detected an unprecedented  
331 increase in ncRNA at both *NTS1* and *NTS2*, observing ~100-fold to ~1000-fold higher levels of  
332 expression in the *Hs* strains compared to *Sc* (Figure 6C and S9C-D). The relative amounts of  
333 *ETS* (external-transcribed spacer, part of the rRNA precursor) transcripts, internally normalized  
334 to *ACT1* mRNA, remained constant between the *Hs* and the *Sc* strains, reflecting a correlation  
335 between rRNA and mRNA levels. As Sir2-dependent transcription at the E-pro has been shown  
336 to regulate rDNA copy number variation<sup>87</sup>, we hypothesize that the human histones in yeast are  
337 responsible for silencing defects in the NTS regions, leading to rDNA instability and locus  
338 amplification. Notably, we found that in the “re-yeastified” strains, the size of the rDNA array was  
339 reduced, and the levels of 18S and 25S rRNAs rebounded to their initial physiological states  
340 (Figure S9E-G).

341 In wild-type yeast the entire rDNA array assembles into a single subnuclear compartment, the  
342 nucleolus, forming a crescent shape structure apposed at the nuclear envelope<sup>92</sup> (Figure 6D,  
343 left schematic). Previous studies have found that nucleolar localization and morphology is  
344 affected by the type of RNA polymerase (I or II) used for the rRNA synthesis<sup>93,94</sup>. Moreover,  
345 nucleolar fragmentation was observed in aged yeast cells<sup>95</sup>, in which elevated ncRNA pol II  
346 dependent transcription<sup>87,91</sup> and variation of copy number at the rDNA locus<sup>83</sup> were also  
347 detected. We thus examined whether NTS de-silencing in the histone-humanized yeasts could  
348 correlate with changes in the organization of the nucleolus. Fluorescent imaging of nuclei, using  
349 a Nop10-GFP nucleolar marker, displayed fragmentation of the nucleolus in ~70% of the *Hs*

350 cells compared to Sc (Figure 6D; see Methods for quantification). These data are consistent  
351 with predictions based on previous studies and support the role of rDNA silencing in maintain  
352 the structure of the nucleolus.

353

### 354 **Discussion**

355 Our electron microscopy data suggest that the size of the *Hs*-NCP in yeast is enlarged. Since  
356 the mass of the protein/histone component of the human nucleosome is actually 0.54%  
357 “smaller” than that of the yeast nucleosome (109.6 kDa vs. 110.2 kDa, respectively), we  
358 conclude that the observed surface increase of the *Hs*-NCP must be due to additional  
359 nucleosome-associated DNA (corresponding to an increase of ~10 bp in the length of the DNA  
360 protected by the NCP, see also MNase-based experiments in Haase et al., co-submission).  
361 Given that both the nucleosome positioning and NRL remain invariant<sup>50</sup>, our current hypothesis  
362 is that the *Hs*-NCP is able to protect ~10 bp more of the yeast linker DNA from MNase activity.  
363 These results support, *in vivo*, the model where predicted stronger interactions between the two  
364 human H2A-H2B dimers relative to yeast favor the binding stability of the human histone  
365 octamer on DNA, underlying fundamental differences in nucleosome packaging between the  
366 two species<sup>52,53,55</sup>.

367

368 Moreover, the Hi-C chromosomal maps showed that the structural effects of histone  
369 humanization go beyond single nucleosome fibers, and suggested that human nucleosomes  
370 allow for more compacted chromatin fibers in yeast (mid-range distances: 20-50 kb). These  
371 observations support a model in which higher nucleosome occupancy, accompanied by lower  
372 DNA accessibility form the basis for the drop in both mRNA and rRNA transcription and to the  
373 impairment of replication origin firing in histone-humanized yeasts. Conversely, lower  
374 humanized-nucleosome occupancy at the tRNA genes was previously shown to increase their  
375 expression<sup>50</sup>.

376 Another intriguing finding is related to the centromeric chromatin. Although the centromeric  
377 histone was not humanized (based on our investigations to date, Cse4, the yeast CenH3  
378 specialized histone, remains unreplaceable by human CENP-A), the peri-centromeric regions  
379 (~50 kb) appeared weakly clustered, suggesting reduced centromeric function - defined by their  
380 ability to stably segregate chromosomes. Moreover, Haase et al.<sup>51</sup> showed that a specific  
381 subset of 8 centromeres (*CEN1-3*, *CEN5*, *CEN9*, *CEN11*, *CEN16*) is more frequently associated  
382 with aneuploidy, and here we found that the same set of peri-centromeres displays a <70%

383 clustering efficiency. Therefore, it is not surprising that histone-humanized yeast lineages often  
384 display chromosomal aneuploidies (see also Haase et al., co-submission).

385

386 *Defect in DNA replication timing.*

387 The absence of a strong early S-phase origin firing in histone-humanized yeast strains resulted  
388 in a noisy temporal replication profile characterized by a multitude of small peaks, reminiscent of  
389 the stochastic/probabilistic model of DNA replication, typical of many eukaryotes, including  
390 humans<sup>96</sup> and some other yeast species<sup>97,98</sup>. The latter model predicts that each origin of  
391 replication follows a unique temporal program that varies stochastically from cell to cell, contrary  
392 to the deterministic one where origins have pre-established timing and frequency of firing<sup>67,73</sup>. In  
393 *S. cerevisiae*, the two models can be reconciled when averaging the heterogeneous replication  
394 kinetics in a large number of cells. This has led to the postulate that the control of replication  
395 timing is deterministic at the level of large chromosomal regions but probabilistic at the level of  
396 single origins<sup>99</sup>. The local chromatin environment at origins was shown to affect origin activity  
397 such as both the introduction of a nucleosome within an ARS<sup>69</sup> and the increased distance  
398 between nucleosomes surrounding origins<sup>70</sup> led to a reduced firing. A more recent study that  
399 performed high-resolution histone chromatin immunoprecipitation followed by deep sequencing  
400 in hydroxyurea (HU) treated cells has found an inverse correlation between nucleosome  
401 occupancy surrounding origins and their firing time, that was dependent on pre-RC formation<sup>100</sup>.  
402 This implies that early origins with a higher frequency of ORC binding display lower nucleosome  
403 occupancy in their surroundings. These observations are particularly relevant to our work, as we  
404 detected an increase in human nucleosome occupancy in the vicinity of the ORC-binding  
405 replication origins (cumulative MNase profile at ARSs, [Figure 4C](#)), accompanied with a global  
406 loss of early firing. These results suggest that the *Hs* nucleosomes may interfere with the  
407 assembly and/or the stability of the pre-RC, which compromises the efficiency of origin firing (in  
408 agreement with previous publications<sup>28,100,101</sup>). On the other hand, we confirmed that DNA  
409 sequences at replication origins are inherently nucleosome-disfavoring<sup>29</sup>, and demonstrated that  
410 this chromatin feature is independent of the NCP's species-specificity, as it was reproduced  
411 ectopically among distantly related eukaryotes (i.e., yeast and human).

412 Intriguingly, humanized Orc4 subunit was shown to cause the loss of ORC's selectivity for  
413 ARSs, leading to its promiscuous and stochastic binding to the constitutively open chromatin of  
414 yeast<sup>102</sup>. Our work showed that the less accessible histone-humanized yeast chromatin loses its  
415 characteristic deterministic replication program. Therefore, we cannot exclude the possibility  
416 that the replication defect in the histone-humanized yeasts maybe due to the increased stability

417 of the *Hs*-NCP that may impinge on the activity of nucleosome/chromatin remodelers.  
418 Alternatively, in light of the remarkable instability of the rDNA locus in the humanized yeasts,  
419 DNA replication of the expanded rDNA locus may require the recruitment of an excess of  
420 limiting replication initiation factors<sup>103</sup>, causing their widespread depletion at replication origins  
421 throughout the rest of the genome.

422

423 *Expansion of the ribosomal DNA locus.*

424 Notably, about half of the rDNA repeats are transcriptionally active at any one time<sup>104,105</sup>. Work  
425 from Ide et al.<sup>106</sup> in budding yeast, established the importance of the extra, untranscribed rDNA  
426 repeats as “protective” against DNA damage in the highly transcribed array. The authors  
427 concluded that while the extra copies of rDNA may not be essential to meet cellular rRNA  
428 demands, rather, they may serve to reduce the transcriptional load on the rDNA to allow  
429 replication-coupled repair and maintain the integrity of this essential locus, especially under  
430 stress conditions. In our case, histone humanization may be seen as a source of endogenous  
431 stress leading to drastic transcriptional dysregulation of the NTS sequences, accompanied by a  
432 remarkable increase in rDNA gene copy number ([Figure 5-6](#)). rDNA expansion appeared  
433 entirely intra-chromosomal (as we failed to detect enrichment in extra-chromosomal rDNA  
434 circles, ERC, [Figure S7](#)), it is thus plausible that rDNA array expansion and concomitant  
435 reduction in rRNA transcripts (RNA polymerase I) represent genomic adjustments necessary to  
436 counterbalance exacerbated transcriptional activity caused by lack of silencing at the NTS (RNA  
437 polymerase II). In other words, the rDNA expansion may serve as a reservoir of RNA pol I  
438 inactive genes to release the overall transcriptional burden and maintain the integrity of this  
439 essential locus (in agreement with Ide et al.<sup>106</sup>). This hypothesis is supported (1) by the rapid  
440 and consistent rDNA size adjustments, when histone genes are swapped from *Sc* to *Hs* and  
441 vice versa [Table S2B-C](#), and (2) by higher nucleosome occupancy at the *rARS*, which may  
442 lower its firing efficiency thus reducing transcription-replication fork collision that leads to DNA  
443 damage response, recombination and ERC formation.

444 We have shown that the expansion of the rDNA locus is due to silencing defects. However, it  
445 remains unclear how human histones interfere with this process given that the Sir2 deacetylated  
446 lysine residues on the H3 and H4 are conserved and that none of the SIR factors (silencing:  
447 Sir2, Sir3, Sir3) nor the RNA I/II/III pol genes were found to be differentially expressed in *Hs* vs.  
448 *Sc* ([Table S4](#)). As often times chromatin modifying enzymes (e.g., SIR factors) require to  
449 contact extensive patches on the surface of the nucleosomes<sup>107</sup>, we cannot exclude that

450 cumulative changes introduced by the *Hs*-NCP may disrupt these interactions and affect their  
451 downstream functions in yeast.

452

453 *A potential interplay between cell size and transcriptional changes.*

454 Biosynthesis of total RNA and proteins increases in proportion to cell size such that their  
455 concentrations remain approximately constant as a cell grows (reviewed in Xie et al.<sup>108</sup>). This  
456 size-dependent transcriptional scaling is thought to ensure constant concentrations of total  
457 mRNA, rRNA and tRNA, to regulate protein synthesis in proportion to cell size (reviewed in  
458 Marguerat and Bahler<sup>109</sup>). An intriguing model for rDNA copy number regulation has proposed  
459 that Sir2 activity (the NTS silencing factor implicated in the stability of the rDNA array) may  
460 decrease after cell enlargement, allowing the increased recombination at the rDNA and its  
461 expansion<sup>110</sup>. Furthermore, recent works by Swaffer et al.<sup>111</sup> and Sun et al.<sup>112</sup> showed that the  
462 increase of RNA polymerase II initiation rate is the major limiting factor for increasing  
463 transcription with cell size in yeasts. Here we hypothesize that the cell size increase observed in  
464 the histone-humanized yeasts<sup>50</sup> may be correlated with the extraordinarily high transcriptional  
465 activity of the RNA pol II at the E-promoter in the NTS regions of the rDNA (Figure S9C-D). Our  
466 current model predicts that the lack of silencing at the NTS will titrate more RNA pol II, causing  
467 its depletion from the free inactive pool whose feedback may eventually translate into both a cell  
468 size increase and rDNA expansion. Experiments to assess both the occupancy of the RNA pol II  
469 and the molecular crowding in the histone-humanized yeast cells are required to validate this  
470 model. We expect to observe that the increased RNA pol II occupancy at the rDNA is  
471 anticorrelated with molecular crowding, given that transcriptional excess does not lead to  
472 functional mRNAs nor rRNA involved in translation.

473

474 Finally, several studies have found that chromatin remodelers (SMC), such as cohesins and  
475 condensins bind many locations in the yeast genome<sup>113,114</sup>, where they play important roles in  
476 the organization of the chromatin. Relevant examples are the origins of replication<sup>115</sup>, the peri-  
477 centromeric regions and the nucleolus (reviewed in Lawrimore and Bloom<sup>116</sup>), where SMCs are  
478 involved in preserving rDNA stability by presumably maintaining silencing at the *cis*-intergenic  
479 sequences<sup>87,91</sup>. As, our results showed an unprecedent increase in non-coding RNA  
480 transcription at the *NTS2*, we cannot exclude the possibility that the human nucleosome in yeast  
481 may affect centromere clustering, firing of replication origins and rDNA stability by altering the  
482 higher-order SMC-dependent organization of the chromatin.

483

484 **Acknowledgments**

485 We thank Sarah French (UVA) for extensive guidance on chromatin preparation for TEM and  
486 the microscopy facility at NYU Langone for electron microscopy training. We thank David  
487 Truong (NYU Tandon), Ran Brosh (NYU Langone), Julien Mozziconacci (MNHN), Jeffrey Smith  
488 (UVA) for helpful discussions and comments on the manuscript, and the entire Boeke lab for  
489 their assistance. This work was supported in part by National Science Foundation grant MCB-  
490 1921641 to J.D.B.

491

492 **Author Contributions**

493 L.L.-S. and J.D.B. designed the research; L.L.-S. and M.A.B.H. performed the experiments and  
494 analyzed the data; L.L.-S., M.A.B.H. and J.D.B. wrote the manuscript.

495

496 **Declaration of Interests**

497 Jef Boeke is a Founder and Director of CDI Labs, Inc., a Founder of Neochromosome, Inc, a  
498 Founder of and Consultant to ReOpen Diagnostics, and serves or served on the Scientific  
499 Advisory Board of the following: Modern Meadow, Inc., Logomix, Inc., Rome Therapeutics, Inc.,  
500 Sample6, Inc., Sangamo, Inc., Tessera Therapeutics, Inc., and the Wyss Institute.

501 The remaining authors declare no competing interests.

502

503

504 **Figure Titles and Legends**

505

506 **Figure 1. Visualizing histone-humanized nucleosome fibers in yeast.**

507 (A) Representative electron microscopy images showing 10 nm nucleosome fibers. Left, wild-  
508 type yeast with native histones (*Saccharomyces cerevisiae*, *Sc*, strain: BY4742; see also [Figure S1](#)). Right, histone-humanized (*Homo sapiens*, *Hs*, strains: yDT92, yDT180 fibers; see also  
509 [Figure S2](#)). (B) Schematic representation of the nucleosome core particle (NCP) with  
510 dimensions in nm. (C) Bee swarm plots showing the average estimated NCP surface area (nm<sup>2</sup>)  
511 in the wild-type (*Sc*) and histone-humanized strains (*Hs*). Median, S.D. and *P* values (\*\*P  
512 <0.0015; n.s. *P* > 0.05) were calculated using a two tailed t-test function ([Table S1](#)). (D)  
513 Boxplots quantifying the difference of the nucleosome fragment length in *Hs* relative to *Sc* (DNA  
514 fragment length analysis of MNase digested chromatin; data from 3 biological replicates:  
515 comparisons of lengths from mono- up to penta-nucleosome fragments are shown by each dot  
516 Haase et al., co-submission).

518

519 **Figure 2. 3D genome organization of histone-humanized chromatin.**

520 (A) Insets of Hi-C contact frequency maps showing chromosome I/V and V underlined by dotted  
521 lines in yeast strains with *Sc* histones vs. *Hs* histones carrying distinct humanization-suppressor  
522 mutations (yDT180 w. *dad1*-E50D and yDT92 w. *scc4*-D65Y). Blue (I/V) and red (V)  
523 chromosomes are plotted on the x and y axis of the maps binned at 5 kb size resolution. Black  
524 arrowheads point at centromere positions, i.e., *CEN4* and *CEN5*. Purple to white color scale  
525 indicates increase in contact frequency (log10). (B) Contact probability (p) in function of the  
526 genomic distance (kb) represents the average decay of the intra-chromosomal contact  
527 frequency between loci with the increment in their genomic distances. Replicates of the strains  
528 in A were plotted together. (C) Comparisons of contact maps in panel A. Log2-ratio maps of  
529 each of the *Hs* strains vs. the *Sc* strain. Color bar indicates contact variation between samples  
530 (log2 ratio 5 kb-binned).

531

532 **Figure 3. Histone humanization leads to de-clustering of yeast centromeres.**

533 (A) Centromere clustering in histone-humanized vs. wild-type yeast using normalized Hi-C  
534 genome maps. Left plots: quantifications of all inter-centromere contacts, plotted in 50 kb-  
535 windows centered on a given centromere (each dot represents the sum of all *trans* contacts a  
536 peri-centromeric region makes with the other 15 peri-centromeres) in the *Hs* (yDT180 *dad1*-  
537 E50D and yDT92 *scc4*-D65Y) strains relative to the corresponding *Sc* from the same

538 experiment (indicated as exp. 1 and 2). Right plot: variations of inter-centromere contacts in *Hs*  
539 vs. *Sc* plotted according to level of chromosome ploidy (aneuploid vs. euploid shown in [Figure](#)  
540 [S3B](#)). **(B)** 3D average representations of the *Sc* and *Hs* corresponding to complete  
541 chromosome-contact maps from [Figure 2A](#). Color code highlight a few chromosomes with either  
542 short or long arms, as well as centromeres (CENs) and telomeres (TELs). **(C)** Schematic model  
543 of Rabl-like organizations of wild-type yeast chromosomes (*Sc* top panel) compared to the  
544 histone-humanized (*Hs* bottom panel) one, showing de-clustering of centromeres. Examples of  
545 chromosome arms (gray lines) anchored at the nuclear membrane through CENs and TELs.  
546

547 **Figure 4. Lack of temporal activation of replication origins on humanized chromosomes.**  
548 **(A)** Each track in the replication timing plots is the average representation of three independent  
549 replicates and shows the sequencing coverage ratio of early-S (HU arrested) synchronized cells  
550 normalized to the G1 (a-factor arrested) non-replicating cells (1 kb-bin size) (see also [Figure](#)  
551 [S4](#)). Replication timing profiles of the wild-type (*Sc*) are shown in blue, while those of the  
552 histone-humanized strain (*Hs*, yDT180 *dad1-E50D*) are in orange. Representative profiles of  
553 chromosome *III* (top left) and chromosome *XII* (bottom left) are shown; positions of all origins  
554 (ARS) are indicated with black circles and arrowheads indicate the early ARS subset. **(B)**  
555 Metaplots of ARS activation were computed on chromosome-by-chromosome ratios between  
556 *Hs* and *Sc* profiles (see also [Figure S5](#)) and plotted in 30 kb ARS-centered windows. **(C)**  
557 Metaplots showing nucleosome occupancy from MNase-sequencing profiles at ARSs in *Hs*  
558 (yDT180 *dad1-E50D* and yDT92 *scc4-D65Y*) compared to *Sc* strains.  
559

560 **Figure 5. Histone humanization leads to the intra-chromosomal expansion of the**  
561 **repeated rDNA array.**

562 **(A)** Estimate rDNA locus sizes (turquoise region on chromosome *XII*) in *Sc* and *Hs* (yDT180  
563 *dad1-E50D*) strains. PFGE of yeast chromosomes digested (+) or not (-) with BamHI and the  
564 corresponding Southern blot with an rDNA specific probe (red). Each “C#” represents an  
565 independent isolated clone of either *Sc* or *Hs* strain (see also [Figure S6A](#)). Left ladder: *H. wingei*  
566 chromosomes. Right ladder: *S. pombe* chromosomes. (\*) indicates chromosome *XII*. PFGE run  
567 specifications: *S. pombe* program for multi-megabase chromosome separation. **(B)** 3D average  
568 representations of the *Sc* and *Hs* Hi-C contact maps (as described in [Figure 3B](#)) where the  
569 estimated position of the rDNA locus is indicated (see also [Figure S6B](#)). Color code highlight a  
570 few short and long chromosomes, as well as centromeres (CENs) and telomeres (TELs). **(C)**  
571 Violin plots showing the estimated rDNA size (Mb) calculated using rDNA-mapped reads (n = #

572 genome sequencing datasets) in *Sc*, histone-humanized (*Hs*: “non-evo.” = non-  
573 evolved/passaged isolates; “40 gen.” and “>100 gen.” = passaged for # generations) and “re-  
574 yeastified” (native *Sc* histones added back to the humanized yeast) strains (see also [Figure S9F](#), [Table S2](#)). *P* values were calculated using the K–S (Kolmogorov–Smirnov) test.  
576

577 **Figure 6. Histone humanization disrupts rDNA silencing and nucleolar structure.**

578 **(A)** Schematic showing the organization of the *RDN1* array (rDNA locus on chromosome *XII*)  
579 and an inset on an example repeat (~9.1 kb-long), showing rRNA genes and regulatory  
580 sequences (*NTS1* and *NTS2* silenced by SIR complex, and Fob1 binding to the Replication  
581 Fork Block, *RFB*). **(B)** Quantification of rRNA levels (18S and 25S) in triplicates of *Sc* and *Hs*  
582 (yDT180 *dad1*-E50D) strains. Total RNA was extracted from equivalent amounts of cells then  
583 quantified on agarose gel using ImageJ (see [Figure S9B](#)). **(C)** RT-qPCR bar plot used to  
584 estimate changes in the transcription of the *NTS1/2* and the rRNA precursor (*ETS*) relative to  
585 the housekeeping mRNA, *ACT1* (see [Figure S9C](#)). **(D)** Left, a simplified representation of  
586 nuclear organization in yeast, where examples of chromosome arms (gray lines) are anchored  
587 at the nuclear membrane through CENs and TELs, and the crescent-shaped nucleolus  
588 (turquoise) are shown. Right, representative microscopy images of *Sc* (strain: yLS110) or *Hs*  
589 (strain: yLS117) yeast nuclei. Nuclear envelope is shown in red (Nup49-RFP) and the nucleolus  
590 in cyan (Nop10-GFP).  
591

592 **Methods**

593 **Resource availability**

594

595 Lead Contact

596 Further information and requests for resources should be directed to Jef D. Boeke  
597 ([jef.boeke@nyulangone.org](mailto:jef.boeke@nyulangone.org)).

598

599 Materials availability

600 Yeast strains generated in this study can be requested directly by contacting the lead contact.  
601 This study did not generate new unique reagents.

602

603 Data and code availability

604 Raw microscopy images were deposited on Mendeley DOI: 10.17632/2j5pzhfm2xm.1  
605 FASTQ files of GWS (HiC datasets and RNA sequencing) in were deposited in the NCBI GEO  
606 database.

607

608 BioProject: PRJNA951416

609 [https://urldefense.com/v3/\\_https://dataview.ncbi.nlm.nih.gov/object/PRJNA951416?reviewer=9gl1a491dj dustacitl4trn5qr\\_!!MXfaZl3!fXrF-4m-0vTACLrafzreljsCgl5nK8nx-v4DBByrn13QNAIgES-GpMkf7kLQEo5QQ\\_d05EHES8O\\_t-QRgCu1Cz5APaqcRSf9Z\\$](https://urldefense.com/v3/_https://dataview.ncbi.nlm.nih.gov/object/PRJNA951416?reviewer=9gl1a491dj dustacitl4trn5qr_!!MXfaZl3!fXrF-4m-0vTACLrafzreljsCgl5nK8nx-v4DBByrn13QNAIgES-GpMkf7kLQEo5QQ_d05EHES8O_t-QRgCu1Cz5APaqcRSf9Z$)

610 <https://dataview.ncbi.nlm.nih.gov/object/PRJNA951416?reviewer=9gl1a491dj dustacitl4trn5qr>

611

612 No new code was generated in this study.

613

614 **Method details**

615 Experimental models and subject details

616 Yeast strains used in this work are listed in the resource [Table S5](#). The deletion of the *FOB1*  
617 coding sequence was achieved using CRISPR-Cas9 in the “shuffle strain” (yMAH666 in which  
618 the encoding yeast histones are exclusively on a centromeric plasmid), and the oligonucleotide  
619 sequences used as gRNA and repair donors are provided in the resource [Table S5](#).

620

621 Media and culture conditions

624 All strains listed were grown in rich medium (Yeast extract Peptone Dextrose (YPD): 1% bacto  
625 peptone (Difco), 1% bacto yeast extract (Difco) and 2% dextrose) liquid or solid (2% agar) at  
626 30°C unless otherwise specified in the methodology below.

627

628 Growth curve assay after “histone re-yeastification”

629 Yeast cultures from three independent isolates of the *Sc* histone strain (yDT67) and 3 of the re-  
630 yeastified *Hs* stains (*Sc* yMAH753/4/5 and *Hs* + *Sc* yMAH756/7/8) were grown to saturation in  
631 YPD liquid medium at 30°C. Yeast cultures in stationary phase were diluted in fresh YPD  
632 medium to an optical density (OD) A600 = 0.07, 200 µl were transferred to 96 well plates and  
633 every minute the BioTek Eon microplate spectrophotometer was programmed to shake the plate  
634 and measure the OD600 every 15 min for a total of 24 h at 30°C. OD600 values were imported  
635 in GraphPad Prism version 9 for Mac OS (GraphPad Software, San Diego, California USA,  
636 [www.graphpad.com](http://www.graphpad.com)) and used to calculate mean and standard deviation for each isolate of  
637 each strain.

638

639 Transmission electron microscopy (TEM) for imaging chromatin fibers

640 For the preparation of chromatin spreads in yeast we followed the published protocol described  
641 by Osheim et al.<sup>117</sup>. We extracted and spread chromatin from log phase yeast cultures (*Sc*  
642 histones: BY4742; *Hs* histones: yDT92, yDT180) grown in YPD with 1M sorbitol at 30°C.  
643 Approximately 10<sup>7</sup> cells were enzymatically lysed using a 1mg/ml Zymolyase 20T (US  
644 biological, Z1000) solution in YPD 1M sorbitol. Chromatin spreading was conducted in a 35 x 10  
645 mm plastic petri dish containing a 0.025% Triton pH 9.1 solution that was incubated at room  
646 temperature and in mild agitation for 45 min. Spreading chromatin was mildly crosslinked with  
647 1/10 [v/v] sucrose-formalin solution (100 mM sucrose, 3.7% formaldehyde Tousimis Research  
648 Corporation, 1008A, with the pH adjusted to 8.8) for an additional ~30 min. Chromatin was  
649 deposited onto the EM carbon grids (Electron Microscopy Sciences, CF300-Cu) by  
650 centrifugation at 7000 x g (Centrifuge: Sorvall LXTR with swinging bucket rotor) for 10 min.  
651 Nucleic acid and protein staining were performed using 4% solutions of Uranyl Acetate (UA)  
652 (Electron Microscopy Sciences cat. 22400-4) and Phosphotungstic acid hydrate (PTA) (Sigma-  
653 Aldrich P4006-10G) in ethanol. Images were acquired using the electron transmission  
654 microscope (FEI Talos 120C TEM) at various resolutions, ranging from 10-kX to 150-kX, at the  
655 NYU Langone Microscopy Laboratory.

656

657 Estimating surface area of the nucleosome core particles (NCPs).

658 Mononucleosome size was measured using images acquired at 200 nm and 100 nm resolution  
659 using ImageJ<sup>118</sup>. Prior measuring of each image was calibrated on the scale bar provide in the  
660 electron microscope image. Raw values can be found in [Table S1](#).

661

662 Hi-C: library preparation

663 Hi-C experiments and data analysis were performed as described<sup>72,119</sup> unless otherwise  
664 indicated in the following method description. Briefly, independent yeast isolates were  
665 inoculated into 5 ml YPD medium and grown overnight at 30°C. The following morning the  
666 overnight cultures were subcultured into 150 ml fresh YPD for ~3 h at 30°C until reaching ~1.2 x  
667 10<sup>9</sup> cells total (~120 OD). Cells were crosslinked using 3% [v/v] formaldehyde for 20 min at  
668 room temperature and then quenched with 350 mM glycine for 15 min at 4°C in mild agitation.  
669 Crosslinked cells were harvested by centrifugation at 1500 x g for 5 min at 4°C, washed twice  
670 with cold fresh medium, and resuspended in 5 ml spheroplast solution (1M sorbitol, 50 mM  
671 potassium phosphate, 5 mM DTT, 250 U zymolyase 100T [US Biological, Z1004]) for 50 min  
672 incubation at 30°C. Spheroplasts were harvested by centrifugation at 2500 x g for 10 min at 4°C,  
673 washed with 10 ml of cold 1 M sorbitol and resuspended in 2 ml of 0.5% SDS, H<sub>2</sub>O at 65°C for  
674 20 min. The crosslinked chromatin was enzymatically fragmented using 125 U of MboI (NEB,  
675 R0147) in a final reaction volume of 3 ml (1X Cutsmart NEBuffer, 0.33% SDS and 2% Triton)  
676 and an incubation at 37°C overnight (up to 16 h). The digested product was centrifuged at  
677 18000 x g for 20 min and the pellet was resuspended in 200 µL cold water. DNA sticky ends  
678 were filled in (to blunt ends) using a biotin-labeled 30 µM dNTP mix (dATP, dGTP, dTTP and  
679 Biotin-14-dCTP Thermo Fischer, 19518018) and Klenow enzyme (NEB, M0210L) at 37°C for 80  
680 min. Biotinylated restriction fragments were re-ligated using 60 Weiss Units of T4 DNA ligase  
681 (Thermo Fischer, EL0014) in 1.2 ml final volume at room temperature for 2 h in mild agitation.  
682 Ligation product was reverse cross-linked by 0.5 mg/mL proteinase K (Thermo Scientific,  
683 EO0492) in 0.5% SDS, 25 mM EDTA buffer at 65°C for 4 h. The un-crosslinked sample was  
684 ethanol precipitated and purified using the large fragment DNA recovery kit (Zymo Research,  
685 D4046). Religated-biotinylated restriction fragments were pulled down using Dynabeads MyOne  
686 Streptavidin C1 magnetic beads (Invitrogen, 65001) according to the manufacture protocol. The  
687 final cleaned-up Hi-C library was used as input material for Illumina sequencing library prep kit  
688 (NEB, E7805) with 6-8 cycles of PCR amplification using KAPA-HiFi (Kapa Biosystems,  
689 KK2602). DNA library was sequenced using an Illumina NextSeq 500 75-cycle high output kit.  
690

691 Hi-C: data processing

692 To generate contact maps: paired-end reads were processed using the HiCLib algorithm<sup>120</sup>  
693 adapted for the *S. cerevisiae* genome. Read-pairs were independently mapped using Bowtie  
694 2<sup>121</sup> (mode: --very-sensitive --rdg 500,3 --rgf 500,3) on the corresponding reference sequence<sup>122</sup>  
695 (S288c available on SGD) indexed for *Mbo*I restriction site. In the contact frequency maps, the  
696 unwanted restriction fragments (RFs) were filtered out (e.g., loops, non-digested fragments,  
697 etc.; as described by Cournac et al.<sup>123</sup>), whereas, the valid RFs were binned into units of fixed  
698 size bins of 5 kb. Bins with a high variance in contact frequency (<1.5 S.D. or 1.5–2 S.D.) were  
699 discarded to remove potential biases resulting from the uneven distribution of restriction sites  
700 and variation in GC% and mappability. The filtered contact maps were normalized using the  
701 sequential component normalization procedure (SCN)<sup>123</sup>. Approximately 10-15 million valid  
702 contacts were used to generate a genomic contact map for each triplicate.

703

704 Contact probability in function of the genomic distance, p(s)

705 The Hi-C contact probability (p) decreases as the genomic distance (s) between restriction  
706 fragments increases<sup>119</sup>. p(s) plots were computed on intra-chromosomal read pairs from which  
707 self-circularizing and uncut events were discarded<sup>123</sup>. The retained reads were log-binned in  
708 function of their distance along chromosome arms, such as the p(s) shows the distribution of the  
709 sum of contacts weighted by both bin-size  $1.1^{(1+bin)}$  and chromosome length (s). Comparison of  
710 the degree of p(s) decay is indicative of a change in polymer state.

711 Log2 ratios of Hi-C contact maps are used to detect contact variation between genomes<sup>119</sup>.

712 Each pairwise comparison was computed on Hi-C normalized maps binned at 5 kb and the  
713 log2-ratio map was Gaussian smoothed (window size of 50 kb).

714 For the 3D representations we used the “Shortest-path Reconstruction in 3D” (ShRec3d)<sup>124</sup>  
715 algorithm as previously described<sup>72</sup>. Finally, the average genome structures were visualized  
716 using PyMol.

717

718 Pulsed-field gel electrophoresis (PFGE) and Southern blotting

719 Chromosomes from stationary yeast cultures (*Sc* histones: BY4741, BY4742, yDT67,  
720 yMAH1242-12447; *Hs* histones: yDT92, yDT180, yLS118-123) were prepared in agar molds  
721 using the Certified Megabase Agarose (Bio-Rad, 1613108), and PFGE was carried out with  
722 running conditions recommended for *S. pombe* chromosomes (BioRad, 170-3633) to maximize  
723 size resolution of the largest chromosomes, as described previously<sup>125</sup>. In agar chromosome  
724 digestion with BamHI (NEB, R0136L) was used to release the entire rDNA locus (~1.5 Mb to ~5  
725 Mb) from chromosome XII. Agar molds treated or not with BamHI were then used for the PFGE

726 and Southern blot. These methods were reported in detail in our previous publication Lazar-  
727 Stefanita et al.<sup>80</sup>. In this specific experiment, we used oligos mapping in the *ETS* and *18S*  
728 sequences of the *RDN37* repeat to generate by PCR a DNA probe (769-bp long), that was  
729 labelled using Klenow Fragment exo- (NEB, M0212L) with Digoxigenin-11-dUTP alkali-stable  
730 (Roche, 11093088910) at 37°C. The labeled and denatured probe was used for the Southern  
731 blot hybridization on a nylon membrane (Pall® 60208 BiodyneTM B Membrane, 60208)  
732 containing the transferred DNA from the PFGE. A primary rabbit anti-DIG antibody (working  
733 concentration 1:4000 in Blocking buffer Odyssey; ABfinity™ Rabbit Monoclonal, 700772)  
734 followed by a secondary antibody (working concentration 1:10000 in Blocking buffer Odyssey;  
735 LIRDye® 680RD Goat anti-Rabbit IgG (H + L), 0.5 mg, 926-68071) were used to specifically  
736 detect the rDNA locus using a LI-COR Odyssey® Imager.

737

738 Exonuclease treatment to detect Extra-chromosomal rDNA circles (ERC)

739 Genomic DNA was extracted from agar plugs (as described above for PFGE chromosome  
740 preparation) using the Zymoclean gel DNA recovery kit (Zymo Research, D4001T) and  
741 successively digested with Exonuclease V (RecBCD, NEB M0345) at 37°C for 3 h. Circular  
742 plasmid (pUC19, NEB N3041S) and sheared (sonicated) genomic DNA were used as digestion  
743 controls.

744

745 Cell cycle synchronization and DNA staining for flow cytometry

746 G1 arrested cells were obtained in triplicate by incubating log-phase growing *Sc* (yDT67) and  
747 *Hs* (yDT180) strains (OD600= 0.3 - 0.5; ~10<sup>7</sup> cells/ml) in YPD supplemented with 0.1 µg/ml a-  
748 factor (Zymo Research, Y1004) for 3 h 30 min (yDT67) or 4 h 30 min (yDT180) at 30°C. Aliquots  
749 of ~2 x 10<sup>7</sup> G1 cells were fixed in 70% ethanol to asses synchronization efficiency; while, the  
750 remainders were centrifuged, washed twice with fresh medium and finally resuspended in  
751 medium containing 200 mM hydroxyurea (HU; Sigma-Aldrich, H8627-25G). These latter  
752 cultures were incubated for 1 h 30 min (yDT67) or 3 h 30 min (yDt180) at 30°C and aliquots  
753 were sampled to microscopically assess for early S-phase arrest.

754 All G1 and HU aliquots (~10<sup>7</sup> cells/replicate, fixed in 70% ethanol) were stored at 4°C overnight  
755 and successively processed for DNA content analysis using flow cytometry. Cells were pelleted  
756 (at 3000 x g for 3 min) and washed three time with 2 ml of RNase solution (10 mM Tris pH 8.0,  
757 15 mM NaCl) before being treated with 0.1 mg/ml RNase A for 3-4 h at 37°C. Cells were  
758 washed once with 50 mM Tris pH 8 and resuspended in labeling solution (1 µM SYTOX Green  
759 in 50 mM Tris pH 8; Thermo Fisher) for 1 h at 4°C protected from light. Before flow cytometry

760 data acquisition, cells were washed three times and resuspended in 50 mM Tris pH 8. Flow  
761 cytometry was performed on a BD Accuri C6 Flow Cytometer (BD CSampler Software) and data  
762 analyzed using FlowJo v10.0.7 software.

763

#### 764 DNA replication timing

765 Each profile of replication timing was generated from three independent clones of *Sc* (yDT67)  
766 and *Hs* (yDT180) strains (see: cell cycle synchronization and DNA staining for flow cytometry)  
767 by deep-sequencing analysis as described previously<sup>73</sup>. Briefly, fractions of replicating and non-  
768 replicating cells were obtained by arresting cells with a-factor for 3 h 30 min (yDT67) or 4 h 30  
769 min (yDT180), then they were washed and released in HU for 1 h 30 min (yDT67) or 3 h 30 min  
770 (yDT180) at 30°C. Synchronization efficiencies were validated by flow cytometry. Pellets of ~6 x  
771 10<sup>8</sup> cells were used to extract genomic DNA using acid-washed beads (Sigma-Aldrich, G8772-  
772 100G) and phenol-chloroform (Thermo Scientific). Library preparation was performed using the  
773 NEBNext Ultra II FS kit (NEB, E7805L) according to the manufacturer's protocol. Resulting  
774 libraries were paired-end deep-sequenced (2 x 36 bp cycles) on NextSeq500 Illumina platform.  
775 Reads were mapped to the corresponding reference genome using Bowtie 2<sup>121</sup> in its --very-  
776 sensitive mode. Profiles of replication timing were generated by normalizing the replicating (S-  
777 phase, HU) sample to the non-replicating (G1, a-factor) sample in 1 kb bins. The resulting ratios  
778 were Gaussian-smoothed (window size of 10 kb) and plotted by genomic coordinate, measuring  
779 variations in DNA copy number as a proxy of replication time.

780

#### 781 Nucleosome maps at replication origins and ribosomal DNA locus

782 We used published MNase-seq datasets<sup>50</sup> to evaluate nucleosome occupancy in the proximity  
783 of replication origins and at the rDNA locus. Genome-wide positions of replication origins,  
784 defined as ORC-binding sites with ARS consensus sequence (total ARS = 251), were obtained  
785 from Eaton et al.<sup>29</sup>. Nucleosome maps were generated following the methods described in the  
786 co-submitted work by Haase et al.

787

#### 788 RNA extraction

789 Total RNA was extracted from 3 independent isolates of *Sc* (yDT67), *Hs* (yDT180, yDT92) and  
790 re-yeastified *Hs* (*Sc* yMAH753/4/5 and *Hs* + *Sc* yMAH756/7/8) strains. Approximately 2 x 10<sup>8</sup>  
791 cells were harvested from mid-log phase cultures (1.5-2 x 10<sup>7</sup> cells/ml) grown in YPD medium at  
792 30°C. Cell pellets were washed in RNase free water and resuspended in RNA lysis buffer (50  
793 mM Tris-HCl pH 8, 100 mM NaCl). Cells were lysed mechanically using acid-washed glass

794 beads (Sigma-Aldrich, G8772-100G) at 4°C. The RNA was extracted by  
795 phenol:chloroform:isoamylalcohol (ThermoFisherScientific, 15593) and ethanol precipitated.  
796 Extractions were treated with DNasel (Agilent, 600031) for 1 h at 37°C and RNA quality was  
797 verified by agarose gel in 1X TAE.

798

799 RNA-based assays

800 Reverse Transcriptase (RT) - quantitative PCR assay. Triplicates of total RNA extractions from  
801 *Sc* (yDT67) and *Hs* (yDT180) strains were used for RT-qPCR reactions with gene specific oligos  
802 (rRNA: *NTS1*, *NTS2*, *ETS1*; mRNA: *ACT1*)<sup>91,126</sup>. The RT reaction was performed according to  
803 the manufacturer protocol SuperScript™ IV Reverse Transcriptase (Invitrogen, 18090050).  
804 Successively, quantitative PCR was performed using the LightCycler® 480 SYBR Green I  
805 Master (Roche, 04887352001) following the standard amplification protocol with 45 cycles in a  
806 multi-well PCR plate 384. Ct values for each replicate were imported in GraphPad Prism version  
807 9 for Mac OS (GraphPad Software, San Diego, California USA, [www.graphpad.com](http://www.graphpad.com)) and used  
808 to calculate mean and standard deviation for each gene in each strain. Raw Ct values can be  
809 found in [Table S3](#).

810 For RNA-seq data and analysis ([Figure S9D](#) and [Table S4](#)) refer to the co-submitted work by  
811 Haase et al.

812

813 Protein tagging and Fluorescent microscopy

814 The organization of the nucleolus within the nucleus was monitored using fluorescently tagged  
815 proteins at their endogenous C-terminus. Nuclear envelope was labeled with mScarlet  
816 (*NUP49::mScarlet-S.p. HIS5*) and the nucleolus with GFP (*NOP10::EGFP-KanMX*) using  
817 reagents that we previously described in Lazar-Stefanita et al.<sup>80</sup> (see strains in the resource  
818 [Table S5](#)). Two independent isolates for each strain, containing either *Sc* or *Hs* histones, were  
819 validated for dual tagging based on their positive emission wavelengths in the GFP (513 nm)  
820 and RFP (605 nm) channels. The resulting strains (*Sc*: yLS110-C1 and yLS110-C3; *Hs*:  
821 yLS117-C1 and yLS117-C2) were grown in SC–His medium to saturation (24 h for yLS110 and  
822 48 h for yLS117) and live cells were imaged in agarose pads prepared in SC–His medium (to  
823 prevent Brownian motion). Imaging was performed on the EVOS M7000 microscope using the  
824 Olympus X-APO 100 Oil, 1.45NA/WD 0.13mm (Oil) objective. Images were acquired as Z-  
825 stacks and visualized as max intensity projections using ImageJ<sup>118</sup>. Different fields of view were  
826 used to count nearly 1000 nuclei (496 for yLS110 and 477 for yLS117) displaying either one  
827 intact nucleolus or many fragmented nucleoli.

828

829 **Quantification and statistical analysis**

830 Information on the number of biological replicates, statistical tests and *P* values are provided in  
831 the Method details and Figure legends.

832

833 **Supplemental Figure Titles and Legends:**

834

835 **Figure S1, related to Main Figure 1.** Nucleosome fibers of wild-type yeast with native histones  
836 (*Saccharomyces cerevisiae*, *Sc*, strain: BY4742). Representative panels showing the 10 nm  
837 fibers at different resolution (scale bars: 100 nm and 200 nm).

838

839 **Figure S2, related to Main Figure 1.** Nucleosome fibers of histone-humanized yeasts (*Homo*  
840 *sapiens*, *Hs*, strains: yDT92, yDT180). Representative panels showing the 10 nm fibers at  
841 different resolution (scale bars: 100 nm and 200 nm).

842

843 **Figure S3, related to Main Figures 2 and 3. Ploidy varies among the histone-humanized**  
844 **strains.**

845 (A) Flow cytometry histograms showing DNA content in histone-humanized yeast strains  
846 stained with SYTOX Green. *Hs* euploid: yDT180 *dad1-E50D*; *Hs* aneuploid: yDT92 *scc4-D65Y*.  
847 (B) Average of chromosome sequencing coverage normalized by the total number of reads.  
848 Aneuploid chromosomes (increased copy number) are shaded in amber. (C) Inter-chromosome  
849 contact variation in the histone-humanized genomes (*Hs*) relative to wild-type (*Sc*). Normalized  
850 Hi-C contact maps (complete maps of the insets shown in [Figure 2A](#)) were used to compute the  
851 ratios between *Hs* and *Sc* strains, which were then plotted according to the level of  
852 chromosome ploidy (aneuploid vs. euploid). The increase of intra-chromosome contacts in the  
853 *Hs* strains ([Figure 2B-C](#)) is likely responsible for the ratio < 1 observed in both the euploid  
854 (yDT180) and in the non-aneuploid chromosomes of yDT92, as an effect of the normalization  
855 process. *P* values were calculated using the K-S (Kolmogorov-Smirnov) test in MATLAB 2018.

856

857 **Figure S4, related to Main Figure 4. Method for mapping replication timing in wild-type**  
858 **and histone-humanized yeasts.**

859 (A) Schematics of the experimental approach used to grow and synchronize yeast cells with  
860 either native (*Sc*) or human (*Hs*, strain: yDT180 *dad1-E50D*) histones in G1 and early S phase.  
861 Star-labeled steps indicate genome-wide sequenced samples used to generate replication  
862 timing profiles. (B) Flow cytometry histograms measuring DNA content of the three  
863 independently synchronized cell cultures in A, stained with SYTOX Green. As expected, no  
864 obvious differences are observed between G1 and early-S phase synchronized cells.

865

866 **Figure S5, related to Main Figure 4. Genome-wide replication timing profiles in wild-type**  
867 **and histone-humanized yeast strains.**

868 Each track in the replication timing plots is the average representation of three independent  
869 replicates and shows the sequencing coverage ratio of early-S (HU) synchronized cells  
870 normalized on the G1 (a-factor) non-replicating cells (1 kb-bin size). Chromosome-by-  
871 chromosome replication timing profiles of the wild-type (*Sc*) are shown in blue, while those of  
872 histone-humanized (*Hs*, yDT180 *dad1*-E50D) are in orange. Origin (ARS) positions are  
873 indicated with gray vertical lines and centromere (CEN) positions are indicated below each plot.  
874

875 **Figure S6, related to Main Figure 5. Histone humanization leads to the expansion of the**  
876 **rDNA array.**

877 (A) Estimated rDNA locus sizes (turquoise region on chromosome *XII*) in independent isolates  
878 of *Sc* (strains: BY4741, yDT67) and *Hs* (strains: yDT92, yDT180) yeasts. PFGE of  
879 chromosomes digested (+) or not (–) with BamHI (left panel) and the corresponding Southern  
880 blot (right panel) with an rDNA specific probe (red). PFGE ladders: *H. wingei* chromosomes  
881 (left) and *S. pombe* chromosomes (right). PFGE run specifications: *S. pombe* program for multi-  
882 megabase chromosome separation. (B) Contact map comparisons showing chromosomes *XII*  
883 and *XIII*. Log2-ratio maps of *Hs* vs. *Sc* strains: yDT180 *dad1*-E50D (left) and yDT92 *scc4*-D65Y  
884 (right). Arrowheads indicate the positions of the two centromeres and the rDNA locus. Color bar  
885 indicates contact variation between samples (log2 ratios 5 kb-binned).  
886

887 **Figure S7, related to Main Figure 5. Histone humanization does not lead to extra-**  
888 **chromosomal rDNA circles.**

889 Agarose gels stained with ethidium bromide showing: (top panel) total genomic DNA extracted  
890 from *Sc* (strains: BY4741, yDT67) and *Hs* (strains: yDT92, yDT180) yeasts and (bottom panel)  
891 after RecBCD treatment. pUC19 circular plasmid and sheared DNA were used as controls. Note  
892 that strains with the *FOB1* gene deleted were also tested and represent negative controls for  
893 extra-chromosomal rDNA circles (ERCs) formation. Red (\*) indicates 2-micron plasmid (~40-60  
894 copies/cell<sup>127</sup>).  
895

896 **Figure S8, related to Main Figure 6. rDNA instability is independent of the replication fork**  
897 **block.**

898 (A) MNase-sequencing coverage profiles at the rDNA locus in *Sc* and *Hs* strains (re-analyzed  
899 data from Truong and Boeke<sup>50</sup>). (B) PFGE of yeast chromosomes in *fob1* $\Delta$  strains (Fob1, rDNA

900 replication fork block-binding protein). *FOB1* was deleted in *Sc* (clones A to F; strains  
901 yMAH1242-12447) followed by histone humanization *Hs* (clones: A# to F#; yLS118-123). Each  
902 lane represents an independent isolated clone. PFGE ladders on the right: *H. wingei* and *S.*  
903 *pombe* chromosomes. (\*) indicates chromosome XII. PFGE run specifications: *S. pombe*  
904 program for multi-megabase chromosome separation.

905

906 **Figure S9, related to Main Figure 6. The epigenetic instability of the rDNA depends on**  
907 **human histones and is reversible.**

908 (A) Schematic showing the organization of a ribosomal DNA repeat unit with rRNA genes (25S,  
909 18S, 5.8S and 5S) and regulatory sequences (*NTS1* and *NTS2* silenced by SIR complex). (B)  
910 Diagram of RNA extractions from triplicates of *Sc* (yDT67) and *Hs* (yDT180 *dad1*-E50D) strains  
911 and agarose gel used for rRNA quantifications in [Figure 6B](#). (C) RT-qPCR bar plot used to  
912 estimate changes in the transcription of the *NTS1/2* ("+" and "-" DNA strands transcribed from  
913 the bidirectional E-promoter located in *NTS1*) and the rRNA precursor (*ETS*) relative to the  
914 control mRNA, *ACT1* (see [Table S3](#)). (D) Total RNA-sequencing coverage tracks at the rDNA  
915 unit in *Sc* and *Hs* strains (see [Table S4](#)). y-axis normalized to read counts per million. (E)  
916 Growth curves in rich media of the "re-yeastified" strains with *dad1*-E50D mutation (without *Hs*  
917 histones, *Sc*: yMAH753-755; *Hs* histones-maintained, *Hs* + *Sc*: yMAH756-758). (F) rDNA read  
918 count of the "re-yeastified" strains in [Figure 5C](#). (G) RNA gel of the "re-yeastified" strains, as  
919 described in panel E (*Sc*: yMAH753-755; *Hs* + *Sc*: yMAH756-758), relative to the wild-type *Sc*  
920 (yDT67) strain.

921

922 **Supplemental Excel Table Titles and Legends:**

923

924 **Table S1, related to Figure 1C. Mononucleosome surface area.** Summary of all measured  
925 mononucleosomes on yeast DNA with *S. cerevisiae* histones (*Sc* strain: BY4742) and human  
926 histones (*Hs* strains: yDT92 and yDT180).

927

928 **Table S2, related to Figure 5C. Estimating rDNA locus size.** (A) rDNA read counts in yeast  
929 strains with either wild-type histones (*Sc*) or human histones (*Hs*). (B) rDNA size after "re-  
930 yeastification" of the chromatin: swap *Hs* histones (pDT109) with the *Sc* histone plasmid  
931 (pDT105 or pDT139). (C) Expansion of the rDNA in independent histone-humanized yeast  
932 isolates carrying distinct humanization suppressor mutations.

933

934 **Table S3, related to Figure 6C and S9C. RT-qPCR measuring NTS transcription.** Raw Ct  
935 values of *NTS1*, *NTS2*, *ETS1* and *ACT1* transcripts in triplicates of yeast strains with *Sc*  
936 histones (strains: BY4741, yDT67) and *Hs* histones (yDT180).

937

938 **Table S4, related to Figure S9D. List of differentially expressed genes.** Combined RNA-  
939 sequencing data analysis from triplicates of yeast strains with *Sc* histones (yDT67) and *Hs*  
940 histones (yDT180). Re-analyzed data from Haase et al.<sup>51</sup>.

941

942

943 **References**

- 944 1. McGhee, J.D., and Felsenfeld, G. (1980). Nucleosome Structure. *Annual Review of*  
945 *Biochemistry* 49, 1115–1156. 10.1146/annurev.bi.49.070180.005343.
- 946 2. Luger, K., Mäder, A.W., Richmond, R.K., Sargent, D.F., and Richmond, T.J. (1997). Crystal  
947 structure of the nucleosome core particle at 2.8 Å resolution. *Nature* 389, 251–260.  
948 10.1038/38444.
- 949 3. Hewish, D.R., and Burgoyne, L.A. (1973). Chromatin sub-structure. The digestion of  
950 chromatin DNA at regularly spaced sites by a nuclear deoxyribonuclease. *Biochemical and*  
951 *Biophysical Research Communications* 52, 504–510. 10.1016/0006-291X(73)90740-7.
- 952 4. Kornberg, R.D., and Lorch, Y. (1999). Twenty-Five Years of the Nucleosome, Fundamental  
953 Particle of the Eukaryote Chromosome. *Cell* 98, 285–294. 10.1016/S0092-8674(00)81958-  
954 3.
- 955 5. Malik, H.S., and Henikoff, S. (2003). Phylogenomics of the nucleosome. *Nat Struct Mol Biol*  
956 10, 882–891. 10.1038/nsb996.
- 957 6. Meluh, P.B., Yang, P., Glowczewski, L., Koshland, D., and Smith, M.M. (1998). Cse4p Is a  
958 Component of the Core Centromere of *Saccharomyces cerevisiae*. *Cell* 94, 607–613.  
959 10.1016/S0092-8674(00)81602-5.
- 960 7. Furuyama, S., and Biggins, S. (2007). Centromere identity is specified by a single  
961 centromeric nucleosome in budding yeast. *Proceedings of the National Academy of*  
962 *Sciences* 104, 14706–14711. 10.1073/pnas.0706985104.
- 963 8. Lawrimore, J., Bloom, K.S., and Salmon, E.D. (2011). Point centromeres contain more than  
964 a single centromere-specific Cse4 (CENP-A) nucleosome. *Journal of Cell Biology* 195, 573–  
965 582. 10.1083/jcb.201106036.
- 966 9. Henikoff, S., Ramachandran, S., Krassovsky, K., Bryson, T.D., Codomo, C.A., Brogaard, K.,  
967 Widom, J., Wang, J.-P., and Henikoff, J.G. (2014). The budding yeast Centromere DNA  
968 Element II wraps a stable Cse4 hemisome in either orientation *in vivo*. *eLife* 3, e01861.  
969 10.7554/eLife.01861.
- 970 10. Cleveland, D.W., Mao, Y., and Sullivan, K.F. (2003). Centromeres and Kinetochores: From  
971 Epigenetics to Mitotic Checkpoint Signaling. *Cell* 112, 407–421. 10.1016/S0092-  
972 8674(03)00115-6.
- 973 11. Cole, H.A., Howard, B.H., and Clark, D.J. (2011). The centromeric nucleosome of budding  
974 yeast is perfectly positioned and covers the entire centromere. *Proceedings of the National*  
975 *Academy of Sciences* 108, 12687–12692. 10.1073/pnas.1104978108.
- 976 12. Jiang, C., and Pugh, B.F. (2009). A compiled and systematic reference map of nucleosome  
977 positions across the *Saccharomyces cerevisiae* genomes. *Genome Biology* 10, R109.  
978 10.1186/gb-2009-10-10-r109.
- 979 13. Lucchini, R., and Sogo, J.M. (1995). Replication of transcriptionally active chromatin. *Nature*  
980 374, 276–280. 10.1038/374276a0.

981 14. Almouzni, G., Clark, D.J., Méchali, M., and Wolffe, A.P. (1990). Chromatin assembly on  
982 replicating DNA in vitro. *Nucleic Acids Res* 18, 5767–5774.

983 15. Xu, M., Long, C., Chen, X., Huang, C., Chen, S., and Zhu, B. (2010). Partitioning of histone  
984 H3-H4 tetramers during DNA replication-dependent chromatin assembly. *Science* 328, 94–  
985 98. 10.1126/science.1178994.

986 16. Verreault, A., Kaufman, P.D., Kobayashi, R., and Stillman, B. (1996). Nucleosome assembly  
987 by a complex of CAF-1 and acetylated histones H3/H4. *Cell* 87, 95–104. 10.1016/s0092-  
988 8674(00)81326-4.

989 17. Kaufman, P.D., Kobayashi, R., Kessler, N., and Stillman, B. (1995). The p150 and p60  
990 subunits of chromatin assembly factor I: a molecular link between newly synthesized  
991 histones and DNA replication. *Cell* 81, 1105–1114. 10.1016/s0092-8674(05)80015-7.

992 18. Hoek, M., and Stillman, B. (2003). Chromatin assembly factor 1 is essential and couples  
993 chromatin assembly to DNA replication in vivo. *Proceedings of the National Academy of  
994 Sciences* 100, 12183–12188. 10.1073/pnas.1635158100.

995 19. Budhavarapu, V.N., Chavez, M., and Tyler, J.K. (2013). How is epigenetic information  
996 maintained through DNA replication? *Epigenetics & Chromatin* 6, 32. 10.1186/1756-8935-6-  
997 32.

998 20. Sauer, P.V., Gu, Y., Liu, W.H., Mattioli, F., Panne, D., Luger, K., and Churchill, M.E. (2018).  
999 Mechanistic insights into histone deposition and nucleosome assembly by the chromatin  
1000 assembly factor-1. *Nucleic Acids Res* 46, 9907–9917. 10.1093/nar/gky823.

1001 21. Thomas, J.O., and Furber, V. (1976). Yeast chromatin structure. *FEBS Letters* 66, 274–280.  
1002 10.1016/0014-5793(76)80521-2.

1003 22. Lohr, D.E. (1981). Detailed analysis of the nucleosomal organization of transcribed DNA in  
1004 yeast chromatin. *Biochemistry* 20, 5966–5972. 10.1021/bi00524a007.

1005 23. Weintraub, H. (1978). The nucleosome repeat length increases during erythropoiesis in the  
1006 chick. *Nucleic Acids Res* 5, 1179–1188. 10.1093/nar/5.4.1179.

1007 24. Perišić, O., Collepardo-Guevara, R., and Schlick, T. (2010). Modeling studies of chromatin  
1008 fiber structure as a function of DNA linker length. *J Mol Biol* 403, 777–802.  
1009 10.1016/j.jmb.2010.07.057.

1010 25. Valouev, A., Johnson, S.M., Boyd, S.D., Smith, C.L., Fire, A.Z., and Sidow, A. (2011).  
1011 Determinants of nucleosome organization in primary human cells. *Nature* 474, 516–520.  
1012 10.1038/nature10002.

1013 26. Rando, O.J., and Chang, H.Y. (2009). Genome-wide views of chromatin structure. *Annu  
1014 Rev Biochem* 78, 245–271. 10.1146/annurev.biochem.78.071107.134639.

1015 27. Lai, W.K.M., and Pugh, B.F. (2017). Understanding nucleosome dynamics and their links to  
1016 gene expression and DNA replication. *Nat Rev Mol Cell Biol* 18, 548–562.  
1017 10.1038/nrm.2017.47.

1018 28. Belsky, J.A., MacAlpine, H.K., Lubelsky, Y., Hartemink, A.J., and MacAlpine, D.M. (2015).  
1019 Genome-wide chromatin footprinting reveals changes in replication origin architecture  
1020 induced by pre-RC assembly. *Genes Dev.* 29, 212–224. 10.1101/gad.247924.114.

1021 29. Eaton, M.L., Galani, K., Kang, S., Bell, S.P., and MacAlpine, D.M. (2010). Conserved  
1022 nucleosome positioning defines replication origins. *Genes Dev.* 24, 748–753.  
1023 10.1101/gad.1913210.

1024 30. Bai, L., and Morozov, A.V. (2010). Gene regulation by nucleosome positioning. *Trends in*  
1025 *Genetics* 26, 476–483. 10.1016/j.tig.2010.08.003.

1026 31. Bowman, G.D., and Poirier, M.G. (2015). Post-Translational Modifications of Histones That  
1027 Influence Nucleosome Dynamics. *Chem. Rev.* 115, 2274–2295. 10.1021/cr500350x.

1028 32. Pokholok, D.K., Harbison, C.T., Levine, S., Cole, M., Hannett, N.M., Lee, T.I., Bell, G.W.,  
1029 Walker, K., Rolfe, P.A., Herbstsheimer, E., et al. (2005). Genome-wide Map of Nucleosome  
1030 Acetylation and Methylation in Yeast. *Cell* 122, 517–527. 10.1016/j.cell.2005.06.026.

1031 33. Schlissel, G., and Rine, J. (2019). The nucleosome core particle remembers its position  
1032 through DNA replication and RNA transcription. *Proceedings of the National Academy of*  
1033 *Sciences* 116, 20605–20611. 10.1073/pnas.1911943116.

1034 34. Kaufman, P.D., and Rando, O.J. (2010). Chromatin as a potential carrier of heritable  
1035 information. *Curr Opin Cell Biol* 22, 284–290. 10.1016/j.ceb.2010.02.002.

1036 35. Campos, E.I., Stafford, J.M., and Reinberg, D. (2014). Epigenetic inheritance: histone  
1037 bookmarks across generations. *Trends in Cell Biology* 24, 664–674.  
1038 10.1016/j.tcb.2014.08.004.

1039 36. Gartenberg, M.R., and Smith, J.S. (2016). The Nuts and Bolts of Transcriptionally Silent  
1040 Chromatin in *Saccharomyces cerevisiae*. *Genetics* 203, 1563–1599.  
1041 10.1534/genetics.112.145243.

1042 37. Imai, S., Armstrong, C.M., Kaeberlein, M., and Guarente, L. (2000). Transcriptional silencing  
1043 and longevity protein Sir2 is an NAD-dependent histone deacetylase. *Nature* 403, 795–800.  
1044 10.1038/35001622.

1045 38. Smith, J.S., Brachmann, C.B., Celic, I., Kenna, M.A., Muhammad, S., Starai, V.J., Avalos,  
1046 J.L., Escalante-Semerena, J.C., Grubmeyer, C., Wolberger, C., et al. (2000). A  
1047 phylogenetically conserved NAD<sup>+</sup>-dependent protein deacetylase activity in the Sir2 protein  
1048 family. *Proceedings of the National Academy of Sciences* 97, 6658–6663.  
1049 10.1073/pnas.97.12.6658.

1050 39. Braunstein, M., Rose, A.B., Holmes, S.G., Allis, C.D., and Broach, J.R. (1993).  
1051 Transcriptional silencing in yeast is associated with reduced nucleosome acetylation. *Genes*  
1052 *Dev.* 7, 592–604. 10.1101/gad.7.4.592.

1053 40. Hoppe, G.J., Tanny, J.C., Rudner, A.D., Gerber, S.A., Danaie, S., Gygi, S.P., and Moazed,  
1054 D. (2002). Steps in Assembly of Silent Chromatin in Yeast: Sir3-Independent Binding of a  
1055 Sir2/Sir4 Complex to Silencers and Role for Sir2-Dependent Deacetylation. *Mol Cell Biol* 22,  
1056 4167–4180. 10.1128/MCB.22.12.4167-4180.2002.

1057 41. Johnson, A., Wu, R., Peetz, M., Gygi, S.P., and Moazed, D. (2013). Heterochromatic Gene  
1058 Silencing by Activator Interference and a Transcription Elongation Barrier\*. *Journal of*  
1059 *Biological Chemistry* 288, 28771–28782. 10.1074/jbc.M113.460071.

1060 42. Behrouzi, R., Lu, C., Currie, M.A., Jih, G., Iglesias, N., and Moazed, D. (2016).  
1061 Heterochromatin assembly by interrupted Sir3 bridges across neighboring nucleosomes.  
1062 *eLife* 5, e17556. 10.7554/eLife.17556.

1063 43. Hecht, A., Laroche, T., Strahl-Bolsinger, S., Gasser, S.M., and Grunstein, M. (1995).  
1064 Histone H3 and H4 N-termini interact with SIR3 and SIR4 proteins: A molecular model for  
1065 the formation of heterochromatin in yeast. *Cell* 80, 583–592. 10.1016/0092-8674(95)90512-  
1066 X.

1067 44. Smith, J.S., and Boeke, J.D. (1997). An unusual form of transcriptional silencing in yeast  
1068 ribosomal DNA. *Genes Dev.* 11, 241–254.

1069 45. Smith, J.S., Brachmann, C.B., Pillus, L., and Boeke, J.D. (1998). Distribution of a Limited  
1070 Sir2 Protein Pool Regulates the Strength of Yeast rDNA Silencing and Is Modulated by  
1071 Sir4p. *Genetics* 149, 1205–1219. 10.1093/genetics/149.3.1205.

1072 46. Kachroo, A.H., Laurent, J.M., Yellman, C.M., Meyer, A.G., Wilke, C.O., and Marcotte, E.M.  
1073 (2015). Systematic humanization of yeast genes reveals conserved functions and genetic  
1074 modularity. *Science* 348, 921–925. 10.1126/science.aaa0769.

1075 47. Hamza, A., Tamppere, E., Kofoed, M., Keong, C., Chiang, J., Giaever, G., Nislow, C., and  
1076 Hieter, P. (2015). Complementation of Yeast Genes with Human Genes as an Experimental  
1077 Platform for Functional Testing of Human Genetic Variants. *Genetics* 201, 1263–1274.  
1078 10.1534/genetics.115.181099.

1079 48. Dunham, M.J., and Fowler, D.M. (2013). Contemporary, yeast-based approaches to  
1080 understanding human genetic variation. *Current Opinion in Genetics & Development* 23,  
1081 658–664. 10.1016/j.gde.2013.10.001.

1082 49. Laurent, J.M., Garge, R.K., Teufel, A.I., Wilke, C.O., Kachroo, A.H., and Marcotte, E.M.  
1083 (2020). Humanization of yeast genes with multiple human orthologs reveals functional  
1084 divergence between paralogs. *PLOS Biology* 18, e3000627. 10.1371/journal.pbio.3000627.

1085 50. Truong, D.M., and Boeke, J.D. (2017). Resetting the yeast epigenome with human  
1086 nucleosomes. *Cell* 171, 1508–1519.e13. 10.1016/j.cell.2017.10.043.

1087 51. Haase, M.A.B., Ólafsson, G., Flores, R.L., Boakye-Ansah, E., Zelter, A., Dickinson, M.S.,  
1088 Lazar-Stefanita, L., Truong, D.M., Asbury, C.L., Davis, T.N., et al. (2023). DASH/Dam1  
1089 complex mutants stabilize ploidy in histone-humanized yeast by weakening kinetochore-  
1090 microtubule attachments. *The EMBO Journal* n/a, e112600. 10.15252/embj.2022112600.

1091 52. White, C.L., Suto, R.K., and Luger, K. (2001). Structure of the yeast nucleosome core  
1092 particle reveals fundamental changes in internucleosome interactions. *EMBO J* 20, 5207–  
1093 5218. 10.1093/emboj/20.18.5207.

1094 53. Tsunaka, Y., Kajimura, N., Tate, S., and Morikawa, K. (2005). Alteration of the nucleosomal  
1095 DNA path in the crystal structure of a human nucleosome core particle. *Nucleic Acids Res*  
1096 33, 3424–3434. 10.1093/nar/gki663.

1097 54. McGinty, R.K., and Tan, S. (2015). Nucleosome Structure and Function. *Chem Rev* 115,  
1098 2255–2273. 10.1021/cr500373h.

1099 55. Mozziconacci, J., and Victor, J.-M. (2003). Nucleosome gaping supports a functional  
1100 structure for the 30nm chromatin fiber. *Journal of Structural Biology* 143, 72–76.  
1101 10.1016/S1047-8477(03)00102-3.

1102 56. Lieberman-Aiden, E., van Berkum, N.L., Williams, L., Imakaev, M., Ragoczy, T., Telling, A.,  
1103 Amit, I., Lajoie, B.R., Sabo, P.J., Dorschner, M.O., et al. (2009). Comprehensive mapping of  
1104 long-range interactions reveals folding principles of the human genome. *Science* 326, 289–  
1105 293. 10.1126/science.1181369.

1106 57. RABL, C. (1885). Über Zellteilung. *Morphologisches Jahrbuch* 10, 214–330.

1107 58. Taddei, A., Schober, H., and Gasser, S.M. (2010). The Budding Yeast Nucleus. *Cold Spring  
1108 Harb Perspect Biol* 2, a000612. 10.1101/cshperspect.a000612.

1109 59. Stinchcomb, D.T., Struhl, K., and Davis, R.W. (1979). Isolation and characterisation of a  
1110 yeast chromosomal replicator. *Nature* 282, 39–43. 10.1038/282039a0.

1111 60. Beach, D., Piper, M., and Shall, S. (1980). Isolation of chromosomal origins of replication in  
1112 yeast. *Nature* 284, 185–187. 10.1038/284185a0.

1113 61. Kearsey, S. (1983). Analysis of sequences conferring autonomous replication in baker's  
1114 yeast. *The EMBO Journal* 2, 1571–1575. 10.1002/j.1460-2075.1983.tb01626.x.

1115 62. Bell, S.P., and Stillman, B. (1992). ATP-dependent recognition of eukaryotic origins of DNA  
1116 replication by a multiprotein complex. *Nature* 357, 128–134. 10.1038/357128a0.

1117 63. Wyrick, J.J., Aparicio, J.G., Chen, T., Barnett, J.D., Jennings, E.G., Young, R.A., Bell, S.P.,  
1118 and Aparicio, O.M. (2001). Genome-Wide Distribution of ORC and MCM Proteins in *S.*  
1119 *cerevisiae*: High-Resolution Mapping of Replication Origins. *Science* 294, 2357–2360.  
1120 10.1126/science.1066101.

1121 64. Li, N., Lam, W.H., Zhai, Y., Cheng, J., Cheng, E., Zhao, Y., Gao, N., and Tye, B.-K. (2018).  
1122 Structure of the origin recognition complex bound to DNA replication origin. *Nature* 559,  
1123 217–222. 10.1038/s41586-018-0293-x.

1124 65. Bell, S.P., and Kaguni, J.M. (2013). Helicase Loading at Chromosomal Origins of  
1125 Replication. *Cold Spring Harb Perspect Biol* 5, a010124. 10.1101/cshperspect.a010124.

1126 66. Remus, D., and Diffley, J.F. (2009). Eukaryotic DNA replication control: Lock and load, then  
1127 fire. *Current Opinion in Cell Biology* 21, 771–777. 10.1016/j.ceb.2009.08.002.

1128 67. Raghuraman, M.K., Winzeler, E.A., Collingwood, D., Hunt, S., Wodicka, L., Conway, A.,  
1129 Lockhart, D.J., Davis, R.W., Brewer, B.J., and Fangman, W.L. (2001). Replication dynamics  
1130 of the yeast genome. *Science* 294, 115–121. 10.1126/science.294.5540.115.

1131 68. Yabuki, N., Terashima, H., and Kitada, K. (2002). Mapping of early firing origins on a  
1132 replication profile of budding yeast. *Genes Cells* 7, 781–789. 10.1046/j.1365-  
1133 2443.2002.00559.x.

1134 69. Simpson, R.T. (1990). Nucleosome positioning can affect the function of a cis-acting DNA  
1135 element in vivo. *Nature* 343, 387–389. 10.1038/343387a0.

1136 70. Lipford, J.R., and Bell, S.P. (2001). Nucleosomes Positioned by ORC Facilitate the Initiation  
1137 of DNA Replication. *Molecular Cell* 7, 21–30. 10.1016/S1097-2765(01)00151-4.

1138 71. Pohl, T.J., Brewer, B.J., and Raghuraman, M.K. (2012). Functional Centromeres Determine  
1139 the Activation Time of Pericentric Origins of DNA Replication in *Saccharomyces cerevisiae*.  
1140 *PLOS Genetics* 8, e1002677. 10.1371/journal.pgen.1002677.

1141 72. Lazar-Stefanita, L., Luo, J., Montagne, R., Thierry, A., Sun, X., Mercy, G., Mozziconacci, J.,  
1142 Koszul, R., and Boeke, J.D. (2022). Karyotype engineering reveals spatio-temporal control  
1143 of replication firing and gene contacts. *Cell Genomics* 2, 100163.  
1144 10.1016/j.xgen.2022.100163.

1145 73. Müller, C.A., Hawkins, M., Retkute, R., Malla, S., Wilson, R., Blythe, M.J., Nakato, R.,  
1146 Komata, M., Shirahige, K., de Moura, A.P.S., et al. (2014). The dynamics of genome  
1147 replication using deep sequencing. *Nucleic Acids Res* 42, e3. 10.1093/nar/gkt878.

1148 74. Berbenetz, N.M., Nislow, C., and Brown, G.W. (2010). Diversity of Eukaryotic DNA  
1149 Replication Origins Revealed by Genome-Wide Analysis of Chromatin Structure. *PLOS*  
1150 *Genetics* 6, e1001092. 10.1371/journal.pgen.1001092.

1151 75. Li, H., Handsaker, B., Wysoker, A., Fennell, T., Ruan, J., Homer, N., Marth, G., Abecasis,  
1152 G., Durbin, R., and 1000 Genome Project Data Processing Subgroup (2009). The  
1153 Sequence Alignment/Map format and SAMtools. *Bioinformatics* 25, 2078–2079.  
1154 10.1093/bioinformatics/btp352.

1155 76. Petes, T.D. (1979). Yeast ribosomal DNA genes are located on chromosome XII. *Proc Natl*  
1156 *Acad Sci U S A* 76, 410–414. 10.1073/pnas.76.1.410.

1157 77. Kobayashi, T., and Sasaki, M. (2017). Ribosomal DNA stability is supported by many ‘buffer  
1158 genes’—introduction to the Yeast rDNA Stability Database. *FEMS Yeast Research* 17,  
1159 fox001. 10.1093/femsyr/fox001.

1160 78. Warner, J.R. (1999). The economics of ribosome biosynthesis in yeast. *Trends in*  
1161 *Biochemical Sciences* 24, 437–440. 10.1016/S0968-0004(99)01460-7.

1162 79. Salim, D., and Gerton, J.L. (2019). Ribosomal DNA instability and genome adaptability.  
1163 *Chromosome Res* 27, 73–87. 10.1007/s10577-018-9599-7.

1164 80. Lazar-Stefanita, L., Luo, J., Haase, M.A.B., Zhang, W., and Boeke, J.D. (2023). Two  
1165 differentially stable rDNA loci coexist on the same chromosome and form a single nucleolus.  
1166 *Proceedings of the National Academy of Sciences* 120, e2219126120.  
1167 10.1073/pnas.2219126120.

1168 81. KOBAYASHI, T. (2014). Ribosomal RNA gene repeats, their stability and cellular  
1169 senescence. *Proc Jpn Acad Ser B Phys Biol Sci* 90, 119–129. 10.2183/pjab.90.119.

1170 82. Sinclair, D.A., and Guarente, L. (1997). Extrachromosomal rDNA Circles— A Cause of  
1171 Aging in Yeast. *Cell* 91, 1033–1042. 10.1016/S0092-8674(00)80493-6.

1172 83. Hotz, M., Thayer, N.H., Hendrickson, D.G., Schinski, E.L., Xu, J., and Gottschling, D.E.  
1173 (2022). rDNA array length is a major determinant of replicative lifespan in budding yeast.  
1174 *Proceedings of the National Academy of Sciences* 119, e2119593119.  
1175 10.1073/pnas.2119593119.

1176 84. Nomura, M., Nogi, Y., and Oakes, M. (2013). Transcription of rDNA in the Yeast  
1177 *Saccharomyces cerevisiae* (Landes Bioscience).

1178 85. Kobayashi, T., Nomura, M., and Horiuchi, T. (2001). Identification of DNA cis elements  
1179 essential for expansion of ribosomal DNA repeats in *Saccharomyces cerevisiae*. *Mol Cell*  
1180 *Biol* 21, 136–147. 10.1128/MCB.21.1.136-147.2001.

1181 86. Kobayashi, T., Heck, D.J., Nomura, M., and Horiuchi, T. (1998). Expansion and contraction  
1182 of ribosomal DNA repeats in *Saccharomyces cerevisiae*: requirement of replication fork  
1183 blocking (Fob1) protein and the role of RNA polymerase I. *Genes Dev.* 12, 3821–3830.  
1184 10.1101/gad.12.24.3821.

1185 87. Kobayashi, T., and Ganley, A.R.D. (2005). Recombination Regulation by Transcription-  
1186 Induced Cohesin Dissociation in rDNA Repeats. *Science* 309, 1581–1584.  
1187 10.1126/science.1116102.

1188 88. Kobayashi, T. (2003). The replication fork barrier site forms a unique structure with Fob1p  
1189 and inhibits the replication fork. *Mol Cell Biol* 23, 9178–9188. 10.1128/MCB.23.24.9178-  
1190 9188.2003.

1191 89. Ide, S., Saka, K., and Kobayashi, T. (2013). Rtt109 Prevents Hyper-Amplification of  
1192 Ribosomal RNA Genes through Histone Modification in Budding Yeast. *PLOS Genetics* 9,  
1193 e1003410. 10.1371/journal.pgen.1003410.

1194 90. Kobayashi, T., Horiuchi, T., Tongaonkar, P., Vu, L., and Nomura, M. (2004). SIR2 regulates  
1195 recombination between different rDNA repeats, but not recombination within individual rRNA  
1196 genes in yeast. *Cell* 117, 441–453. 10.1016/s0092-8674(04)00414-3.

1197 91. Pal, S., Postnikoff, S.D., Chavez, M., and Tyler, J.K. (2018). Impaired cohesion and  
1198 homologous recombination during replicative aging in budding yeast. *Sci Adv* 4.  
1199 10.1126/sciadv.aaq0236.

1200 92. Dvorkin, N., Clark, M.W., and Hamkalo, B.A. (1991). Ultrastructural localization of nucleic  
1201 acid sequences in *Saccharomyces cerevisiae* nucleoli. *Chromosoma* 100, 519–523.  
1202 10.1007/BF00352202.

1203 93. Oakes, M., Aris, J.P., Brockenbrough, J.S., Wai, H., Vu, L., and Nomura, M. (1998).  
1204 Mutational Analysis of the Structure and Localization of the Nucleolus in the Yeast  
1205 *Saccharomyces cerevisiae*. *Journal of Cell Biology* 143, 23–34. 10.1083/jcb.143.1.23.

1206 94. Oakes, M., Nogi, Y., Clark, M.W., and Nomura, M. (1993). Structural alterations of the  
1207 nucleolus in mutants of *Saccharomyces cerevisiae* defective in RNA polymerase I.  
1208 *Molecular and Cellular Biology* 13, 2441–2455. 10.1128/mcb.13.4.2441-2455.1993.

1209 95. Sinclair, D.A., Mills, K., and Guarente, L. (1997). Accelerated Aging and Nucleolar  
1210 Fragmentation in Yeast *sgs1* Mutants. *Science* 277, 1313–1316.  
1211 10.1126/science.277.5330.1313.

1212 96. Wang, W., Klein, K.N., Proesmans, K., Yang, H., Marchal, C., Zhu, X., Borrman, T., Hastie,  
1213 A., Weng, Z., Bechhoefer, J., et al. (2021). Genome-wide mapping of human DNA  
1214 replication by optical replication mapping supports a stochastic model of eukaryotic  
1215 replication. *Molecular Cell* 81, 2975-2988.e6. 10.1016/j.molcel.2021.05.024.

1216 97. Patel, P.K., Arcangioli, B., Baker, S.P., Bensimon, A., and Rhind, N. (2006). DNA replication  
1217 origins fire stochastically in fission yeast. *Mol. Biol. Cell* 17, 308–316. 10.1091/mbc.E05-07-  
1218 0657.

1219 98. Czajkowsky, D.M., Liu, J., Hamlin, J.L., and Shao, Z. (2008). DNA Combing Reveals  
1220 Intrinsic Temporal Disorder in the Replication of Yeast Chromosome VI. *Journal of  
1221 Molecular Biology* 375, 12–19. 10.1016/j.jmb.2007.10.046.

1222 99. Tuduri, S., Tourrière, H., and Pasero, P. (2010). Defining replication origin efficiency using  
1223 DNA fiber assays. *Chromosome Res* 18, 91–102. 10.1007/s10577-009-9098-y.

1224 100. Rodriguez, J., Lee, L., Lynch, B., and Tsukiyama, T. (2017). Nucleosome occupancy as  
1225 a novel chromatin parameter for replication origin functions. *Genome Res* 27, 269–277.  
1226 10.1101/gr.209940.116.

1227 101. Semple, J.W., Da-Silva, L.F., Jervis, E.J., Ah-Kee, J., Al-Attar, H., Kummer, L., Heikkila,  
1228 J.J., Pasero, P., and Duncker, B.P. (2006). An essential role for Orc6 in DNA replication  
1229 through maintenance of pre-replicative complexes. *The EMBO Journal* 25, 5150–5158.  
1230 10.1038/sj.emboj.7601391.

1231 102. Lee, C.S.K., Cheung, M.F., Li, J., Zhao, Y., Lam, W.H., Ho, V., Rohs, R., Zhai, Y.,  
1232 Leung, D., and Tye, B.-K. (2021). Humanizing the yeast origin recognition complex. *Nat  
1233 Commun* 12, 33. 10.1038/s41467-020-20277-y.

1234 103. Mantiero, D., Mackenzie, A., Donaldson, A., and Zegerman, P. (2011). Limiting  
1235 replication initiation factors execute the temporal programme of origin firing in budding  
1236 yeast. *The EMBO Journal* 30, 4805–4814. 10.1038/emboj.2011.404.

1237 104. Conconi, A., Widmer, R.M., Koller, T., and Sogo, J.M. (1989). Two different chromatin  
1238 structures coexist in ribosomal RNA genes throughout the cell cycle. *Cell* 57, 753–761.

1239 105. French, S.L., Osheim, Y.N., Cioci, F., Nomura, M., and Beyer, A.L. (2003). In  
1240 Exponentially Growing *Saccharomyces cerevisiae* Cells, rRNA Synthesis Is Determined by  
1241 the Summed RNA Polymerase I Loading Rate Rather than by the Number of Active Genes.  
1242 *Molecular and Cellular Biology* 23, 1558–1568. 10.1128/MCB.23.5.1558-1568.2003.

1243 106. Ide, S., Miyazaki, T., Maki, H., and Kobayashi, T. (2010). Abundance of Ribosomal RNA  
1244 Gene Copies Maintains Genome Integrity. *Science* 327, 693–696.  
1245 10.1126/science.1179044.

1246 107. Armache, K.-J., Garlick, J.D., Canzio, D., Narlikar, G.J., and Kingston, R.E. (2011).  
1247 Structural basis of silencing: Sir3 BAH domain in complex with a nucleosome at 3.0 Å  
1248 resolution. *Science* 334, 977–982. 10.1126/science.1210915.

1249 108. Xie, S., Swaffer, M., and Skotheim, J.M. (2022). Eukaryotic Cell Size Control and Its  
1250 Relation to Biosynthesis and Senescence. *Annual Review of Cell and Developmental  
1251 Biology* 38, 291–319. 10.1146/annurev-cellbio-120219-040142.

1252 109. Marguerat, S., and Bähler, J. (2012). Coordinating genome expression with cell size.  
1253 *Trends in Genetics* 28, 560–565. 10.1016/j.tig.2012.07.003.

1254 110. Pérez-Ortín, J.E., Mena, A., Barba-Aliaga, M., Singh, A., Chávez, S., and García-  
1255 Martínez, J. (2021). Cell volume homeostatically controls the rDNA repeat copy number and  
1256 rRNA synthesis rate in yeast. *PLoS Genet* 17, e1009520. 10.1371/journal.pgen.1009520.

1257 111. Swaffer, M.P., Marinov, G.K., Zheng, H., Tsui, C.Y., Jones, A.W., Greenwood, J.,  
1258 Kundaje, A., Greenleaf, W.J., Reyes-Lamothe, R., and Skotheim, J.M. (2022). RNA  
1259 polymerase II dynamics and mRNA stability feedback scale mRNA in proportion to cell size.  
1260 2021.09.20.461005. 10.1101/2021.09.20.461005.

1261 112. Sun, X.-M., Bowman, A., Priestman, M., Bertaux, F., Martinez-Segura, A., Tang, W.,  
1262 Whilding, C., Dormann, D., Shahrezaei, V., and Marguerat, S. (2020). Size-Dependent  
1263 Increase in RNA Polymerase II Initiation Rates Mediates Gene Expression Scaling with Cell  
1264 Size. *Current Biology* 30, 1217–1230.e7. 10.1016/j.cub.2020.01.053.

1265 113. Glynn, E.F., Megee, P.C., Yu, H.-G., Mistrot, C., Unal, E., Koshland, D.E., DeRisi, J.L.,  
1266 and Gerton, J.L. (2004). Genome-Wide Mapping of the Cohesin Complex in the Yeast  
1267 *Saccharomyces cerevisiae*. *PLOS Biol* 2, e259. 10.1371/journal.pbio.0020259.

1268 114. Wang, B.-D., Eyre, D., Basrai, M., Lichten, M., and Strunnikov, A. (2005). Condensin  
1269 Binding at Distinct and Specific Chromosomal Sites in the *Saccharomyces cerevisiae*  
1270 Genome. *Mol. Cell. Biol.* 25, 7216–7225. 10.1128/MCB.25.16.7216-7225.2005.

1271 115. Guillou, E., Ibarra, A., Coulon, V., Casado-Vela, J., Rico, D., Casal, I., Schwob, E.,  
1272 Losada, A., and Méndez, J. (2010). Cohesin organizes chromatin loops at DNA replication  
1273 factories. *Genes Dev* 24, 2812–2822. 10.1101/gad.608210.

1274 116. Lawrimore, C.J., and Bloom, K. (2019). Common Features of the Pericentromere and  
1275 Nucleolus. *Genes (Basel)* 10, 1029. 10.3390/genes10121029.

1276 117. Osheim, Y.N., French, S.L., Sikes, M.L., and Beyer, A.L. (2008). Electron Microscope  
1277 Visualization of RNA Transcription and Processing in *Saccharomyces cerevisiae* by Miller  
1278 Chromatin Spreading. In *The Nucleus: Volume 2: Chromatin, Transcription, Envelope,  
1279 Proteins, Dynamics, and Imaging Methods in Molecular Biology*, R. Hancock, ed. (Humana  
1280 Press), pp. 55–69. 10.1007/978-1-60327-461-6\_4.

1281 118. Schneider, C.A., Rasband, W.S., and Eliceiri, K.W. (2012). NIH Image to ImageJ: 25  
1282 years of image analysis. *Nat Methods* 9, 671–675. 10.1038/nmeth.2089.

1283 119. Lazar-Stefanita, L., Scolari, V.F., Mercy, G., Muller, H., Guérin, T.M., Thierry, A.,  
1284 Mozziconacci, J., and Koszul, R. (2017). Cohesins and condensins orchestrate the 4D  
1285 dynamics of yeast chromosomes during the cell cycle. *EMBO J* 36, 2684–2697.  
1286 10.15252/embj.201797342.

1287 120. Imakaev, M., Fudenberg, G., McCord, R.P., Naumova, N., Goloborodko, A., Lajoie, B.R.,  
1288 Dekker, J., and Mirny, L.A. (2012). Iterative correction of Hi-C data reveals hallmarks of  
1289 chromosome organization. *Nat Methods* 9, 999–1003. 10.1038/nmeth.2148.

1290 121. Langmead, B., and Salzberg, S.L. (2012). Fast gapped-read alignment with Bowtie 2.  
1291 *Nat. Methods* 9, 357–359. 10.1038/nmeth.1923.

1292 122. Engel, S.R., Dietrich, F.S., Fisk, D.G., Binkley, G., Balakrishnan, R., Costanzo, M.C.,  
1293 Dwight, S.S., Hitz, B.C., Karra, K., Nash, R.S., et al. (2014). The reference genome  
1294 sequence of *Saccharomyces cerevisiae*: then and now. *G3 (Bethesda)* 4, 389–398.  
1295 10.1534/g3.113.008995.

1296 123. Cournac, A., Marie-Nelly, H., Marbouty, M., Koszul, R., and Mozziconacci, J. (2012).  
1297 Normalization of a chromosomal contact map. *BMC Genomics* 13, 436. 10.1186/1471-2164-  
1298 13-436.

1299 124. Lesne, A., Riposo, J., Roger, P., Cournac, A., and Mozziconacci, J. (2014). 3D genome  
1300 reconstruction from chromosomal contacts. *Nat Methods* 11, 1141–1143.  
1301 10.1038/nmeth.3104.

1302 125. Luo, J., Sun, X., Cormack, B.P., and Boeke, J.D. (2018). Karyotype engineering by  
1303 chromosome fusion leads to reproductive isolation in yeast. *Nature* 560, 392–396.  
1304 10.1038/s41586-018-0374-x.

1305 126. Wei, T., Najmi, S.M., Liu, H., Peltonen, K., Kucerova, A., Schneider, D.A., and Laiho, M.  
1306 (2018). Small-Molecule Targeting of RNA Polymerase I Activates a Conserved Transcription  
1307 Elongation Checkpoint. *Cell Reports* 23, 404–414. 10.1016/j.celrep.2018.03.066.

1308 127. Broach, J.R. (1982). The yeast plasmid 2μ circle. *Cell* 28, 203–204. 10.1016/0092-  
1309 8674(82)90337-3.

1310

## Combined Figures and Legends for Manuscript:

### Title:

Humanized nucleosomes reshape replication initiation and rDNA/nucleolar integrity in yeast.

**Authors:** Luciana Lazar-Stefanita<sup>1\*</sup>, Max A. B. Haase<sup>1,2</sup>, Jef D. Boeke<sup>1,3\*</sup>

Lead Contact: Jef D. Boeke, [jef.boeke@nyulangone.org](mailto:jef.boeke@nyulangone.org)

### Affiliations:

<sup>1</sup>Institute for Systems Genetics and Department of Biochemistry and Molecular Pharmacology, NYU Langone Health, New York, NY 10016, USA

<sup>2</sup>Vilcek Institute of Graduate Biomedical Sciences at NYU School of Medicine, NY 10016, USA

<sup>3</sup>Department of Biomedical Engineering, NYU Tandon School of Engineering, Brooklyn, NY 11201, USA

\*Correspondence: L.L.-S., [luciana.lazarstefanita@nyulangone.org](mailto:luciana.lazarstefanita@nyulangone.org), J.D.B. [jef.boeke@nyulangone.org](mailto:jef.boeke@nyulangone.org)

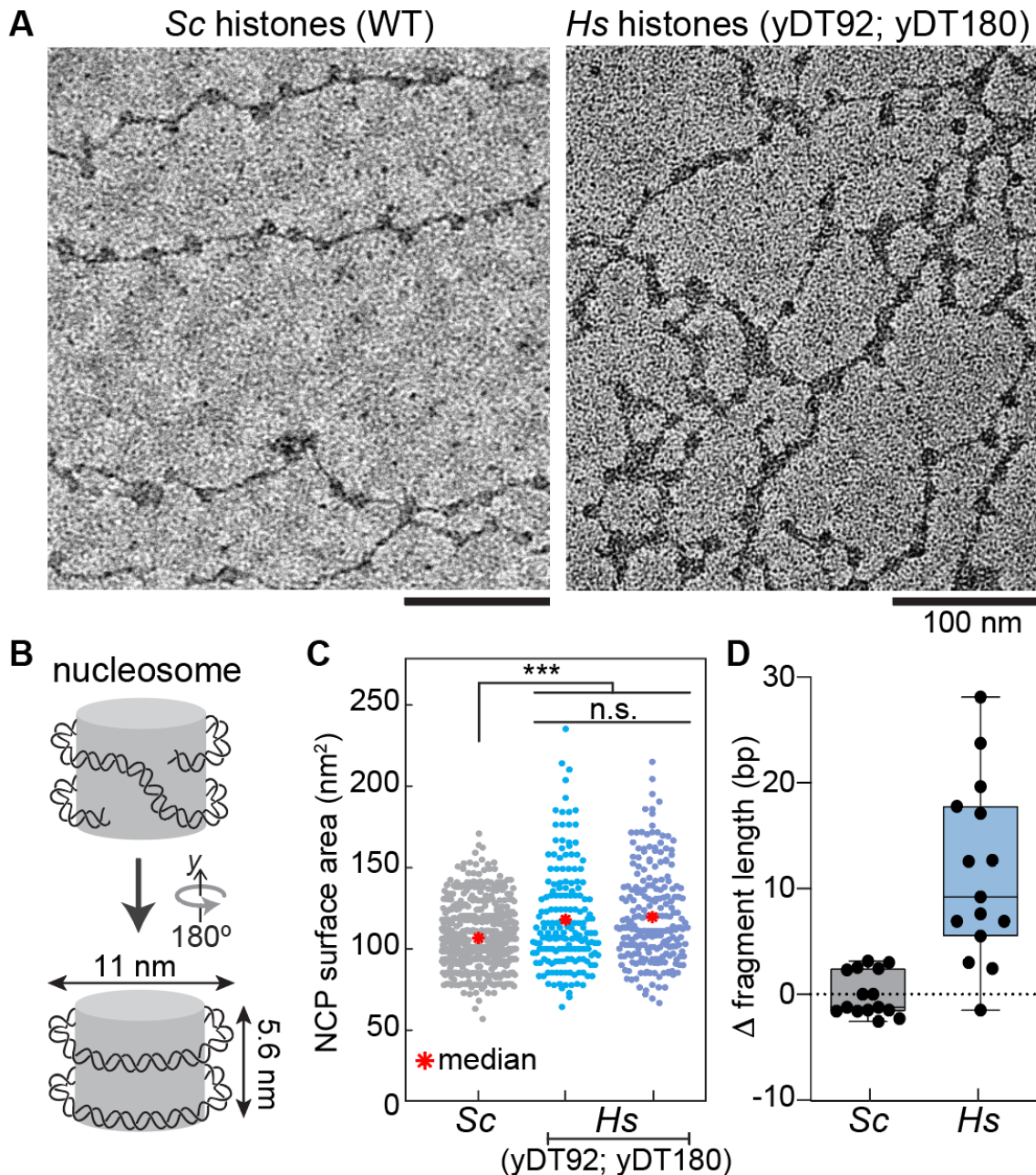


**Figure 1. Visualizing histone-humanized nucleosome fibers in yeast.**

(A) Representative electron microscopy images showing 10 nm nucleosome fibers. Left, wild-type yeast with native histones (*Saccharomyces cerevisiae*, *Sc*, strain: BY4742; see also Figure S1). Right, histone-humanized (*Homo sapiens*, *Hs*, strains: yDT92, yDT180 fibers; see also Figure S2). (B) Schematic representation of the nucleosome core particle (NCP) with dimensions in nm. (C) Bee swarm plots showing the average estimated NCP surface area ( $\text{nm}^2$ ) in the wild-type (*Sc*) and histone-humanized strains (*Hs*). Median, S.D. and  $P$  values (\*\* $P$  < 0.001, n.s. = not significant). (D) Box plot of  $\Delta$  fragment length (bp) for *Sc* and *Hs*.  $\Delta$  fragment length is calculated as the difference between the average estimated NCP surface area in *Hs* and *Sc*.

<0.0015; n.s.  $P > 0.05$ ) were calculated using a two tailed t-test function (Table S1). (D) Boxplots quantifying the difference of the nucleosome fragment length in *Hs* relative to *Sc* (DNA fragment length analysis of MNase digested chromatin; data from 3 biological replicates: comparisons of lengths from mono- up to penta-nucleosome fragments are shown by each dot Haase et al., co-submission).

Sc histones (WT; BY4742)

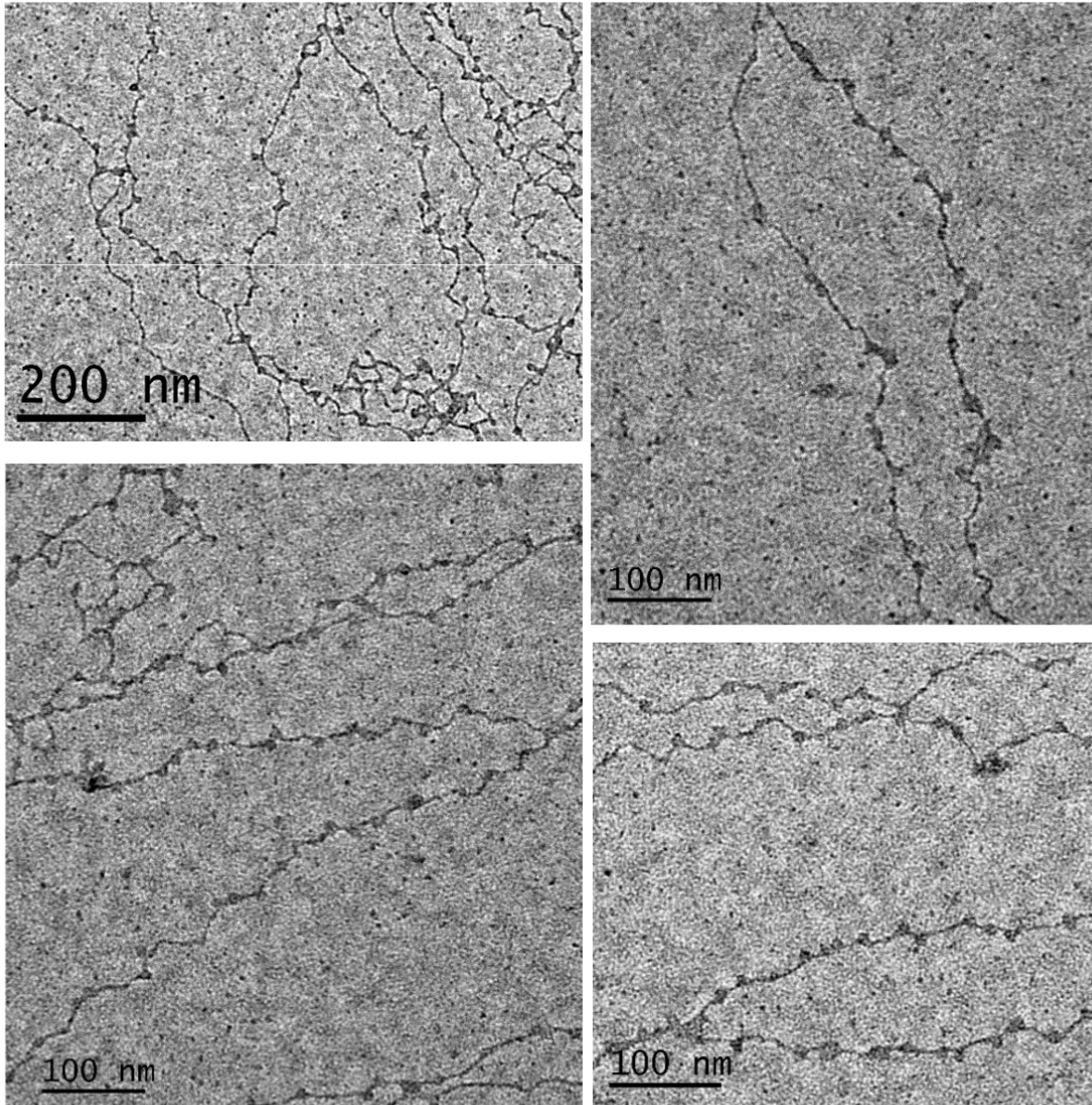


**Figure S1, related to Main Figure 1.** Nucleosome fibers of wild-type yeast with native histones (*Saccharomyces cerevisiae*, Sc, strain: BY4742). Representative panels showing the 10 nm fibers at different resolution (scale bars: 100 nm and 200 nm).

*Hs* histones (yDT92; yDT180)

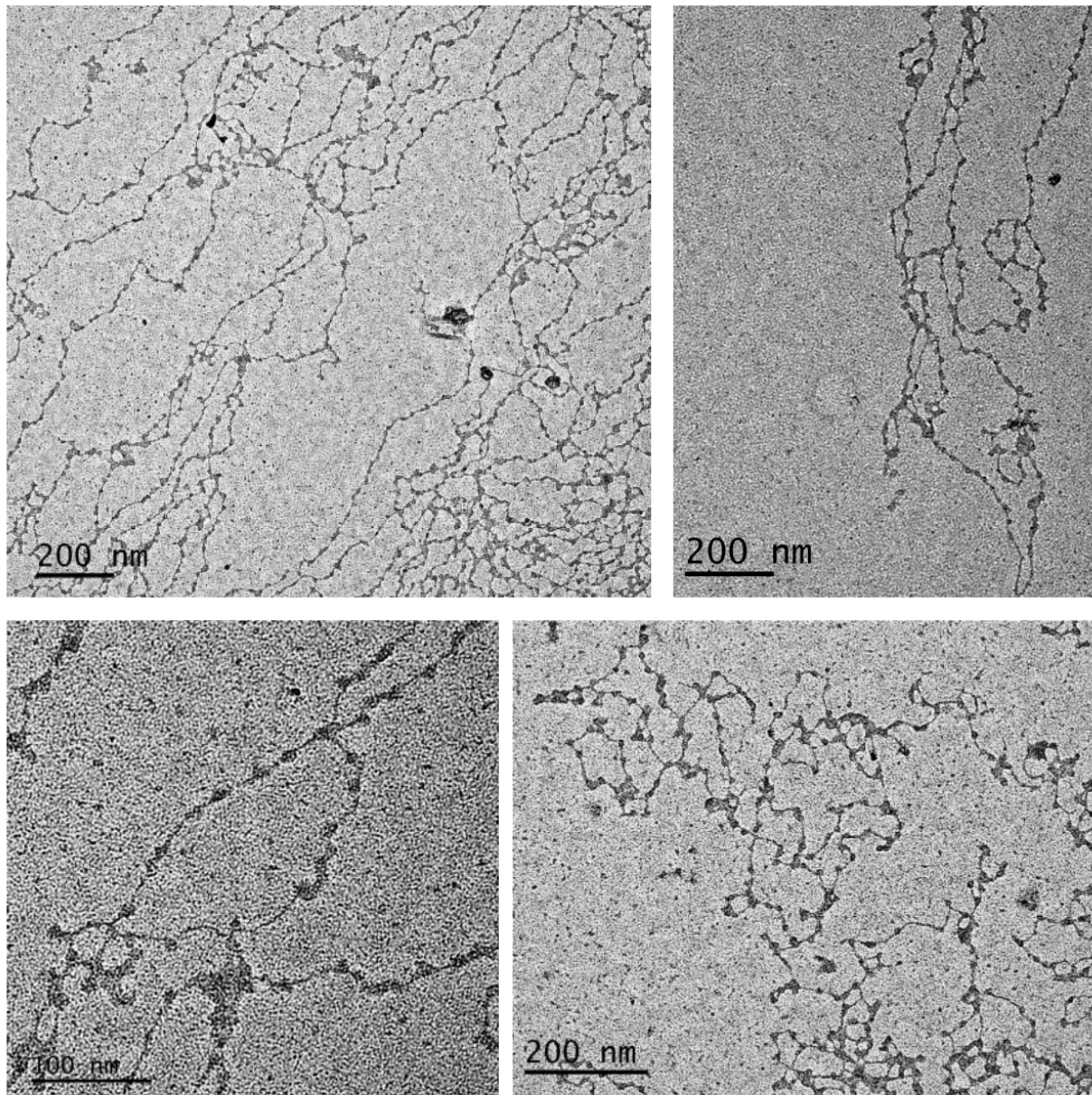


**Figure S2, related to Main Figure 1.** Nucleosome fibers of histone-humanized yeasts (*Homo sapiens*, *Hs*, strains: yDT92, yDT180). Representative panels showing the 10 nm fibers at different resolution (scale bars: 100 nm and 200 nm).

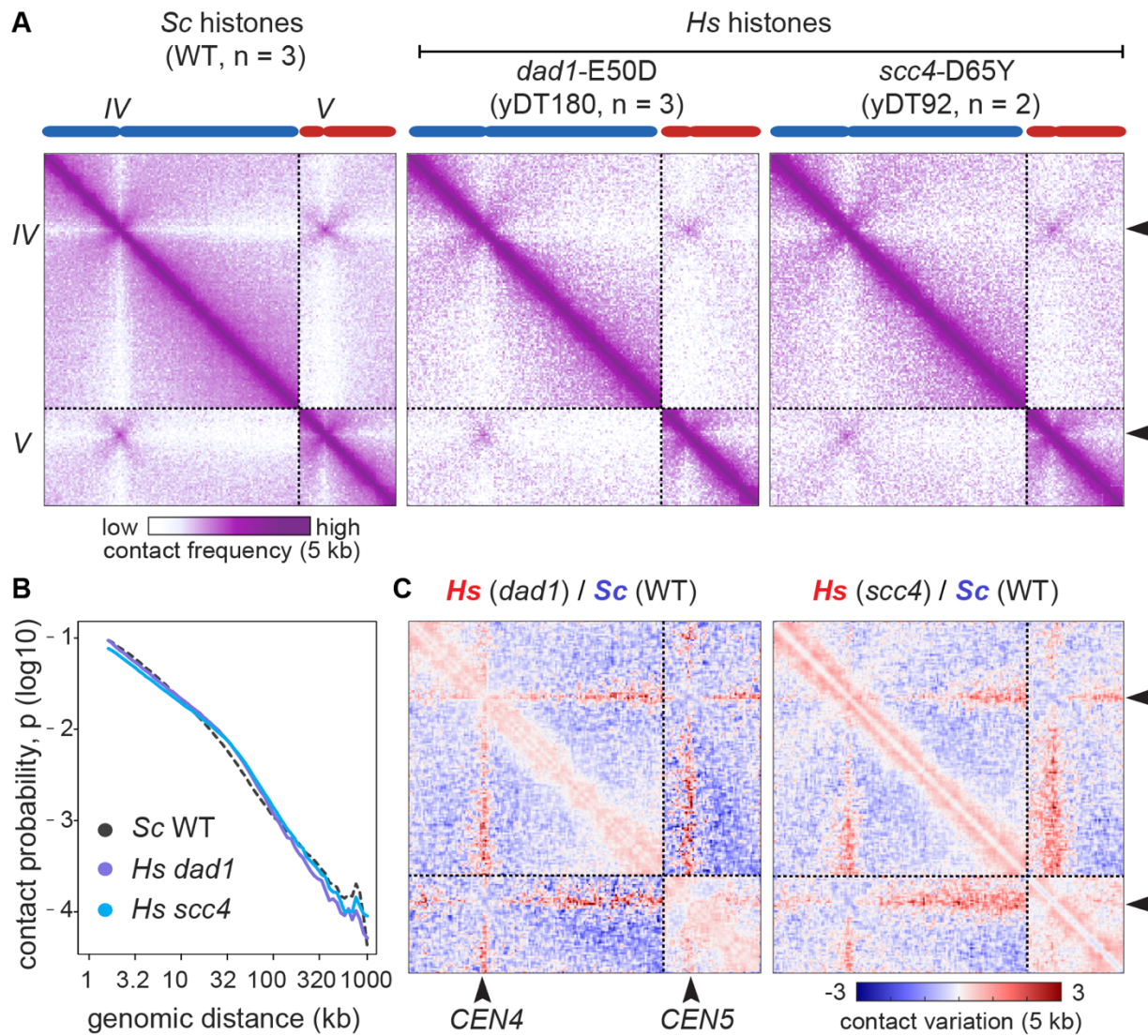


**Figure 2. 3D genome organization of histone-humanized chromatin.**

**(A)** Insets of Hi-C contact frequency maps showing chromosome /IV and V underlined by dotted lines in yeast strains with *Sc* histones vs. *Hs* histones carrying distinct humanization-suppressor mutations (yDT180 w. *dad1*-E50D and yDT92 w. *scc4*-D65Y). Blue (/IV) and red (V) chromosomes are plotted on the x and y axis of the maps binned at 5 kb size resolution. Black arrowheads point at centromere positions, i.e., *CEN4* and *CEN5*. Purple to white color scale indicates increase in contact frequency (log10). **(B)** Contact probability ( $p$ ) in function of the genomic distance (kb) represents the average decay of the intra-chromosomal contact frequency between loci with the increment in their genomic distances. Replicates of the strains in A were plotted together. **(C)** Comparisons of contact maps in panel A. Log2-ratio maps of

each of the *Hs* strains vs. the *Sc* strain. Color bar indicates contact variation between samples (log2 ratio 5 kb-binned).

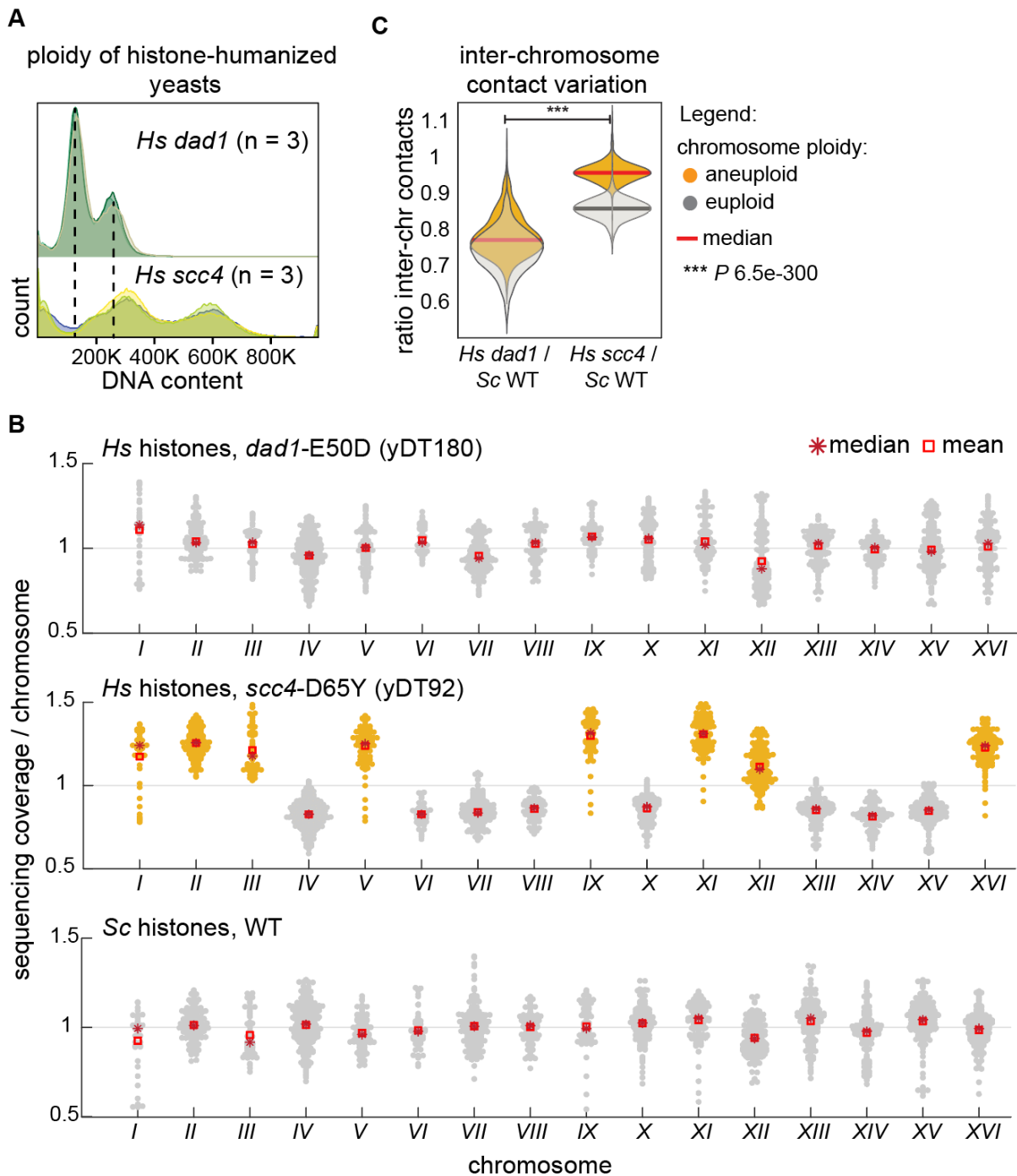


**Figure S3, related to Main Figures 2 and 3. Ploidy varies among the histone-humanized strains.**

**(A)** Flow cytometry histograms showing DNA content in histone-humanized yeast strains stained with SYTOX Green. *Hs* euploid: yDT180 *dad1-E50D*; *Hs* aneuploid: yDT92 *scc4-D65Y*.

**(B)** Average of chromosome sequencing coverage normalized by the total number of reads. Aneuploid chromosomes (increased copy number) are shaded in amber. **(C)** Inter-chromosome

contact variation in the histone-humanized genomes (*Hs*) relative to wild-type (*Sc*). Normalized Hi-C contact maps (complete maps of the insets shown in [Figure 2A](#)) were used to compute the ratios between *Hs* and *Sc* strains, which were then plotted according to the level of chromosome ploidy (aneuploid vs. euploid). The increase of intra-chromosome contacts in the *Hs* strains ([Figure 2B-C](#)) is likely responsible for the ratio  $< 1$  observed in both the euploid (yDT180) and in the non-aneuploid chromosomes of yDT92, as an effect of the normalization process. *P* values were calculated using the K-S (Kolmogorov–Smirnov) test in MATLAB 2018.

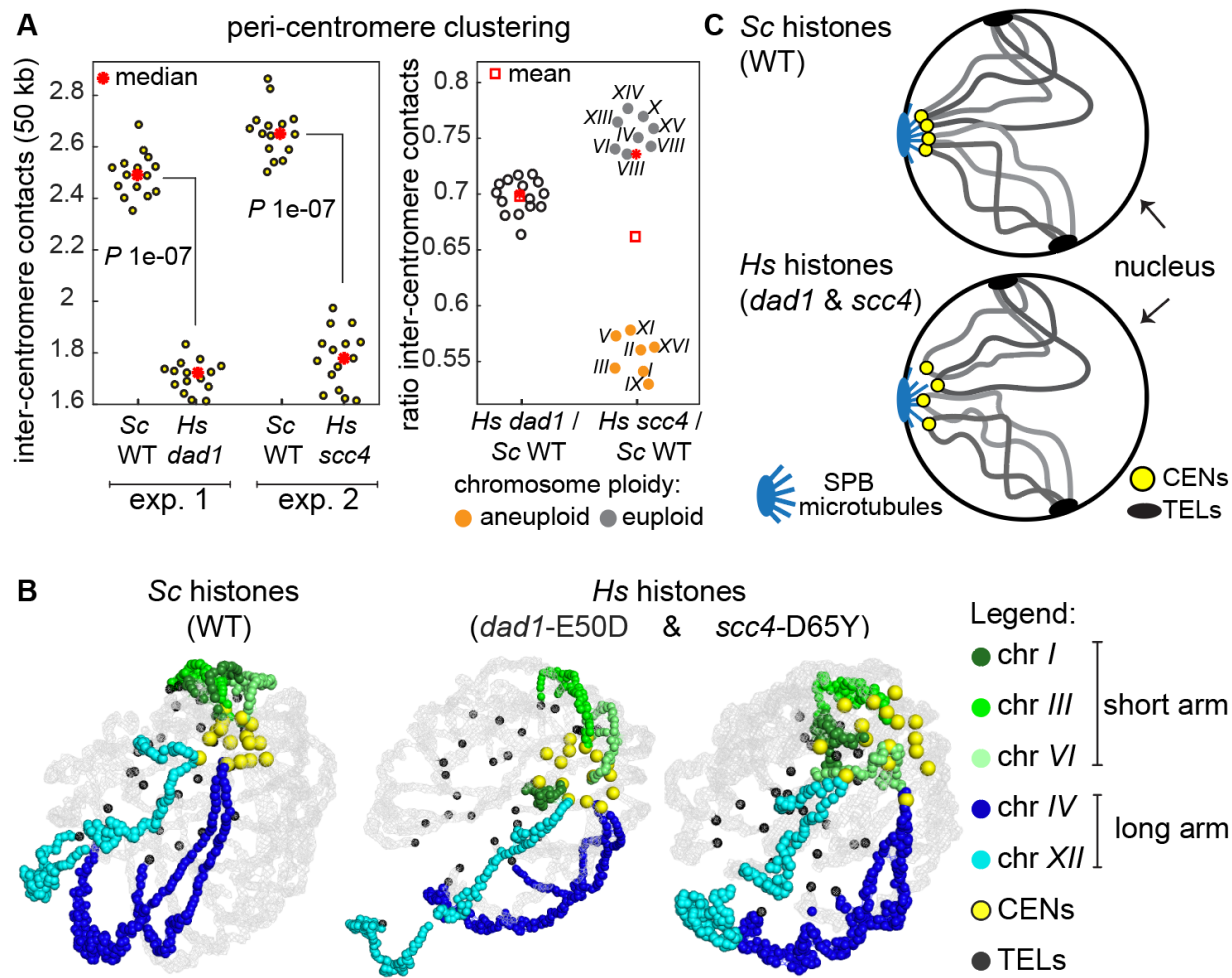


**Figure 3. Histone humanization leads to de-clustering of yeast centromeres.**

**(A)** Centromere clustering in histone-humanized vs. wild-type yeast using normalized Hi-C genome maps. Left plots: quantifications of all inter-centromere contacts, plotted in 50 kb-windows centered on a given centromere (each dot represents the sum of all *trans* contacts a peri-centromeric region makes with the other 15 peri-centromeres) in the *Hs* (*yDT180 dad1-E50D* and *yDT92 scc4-D65Y*) strains relative to the corresponding *Sc* from the same experiment (indicated as exp. 1 and 2). Right plot: variations of inter-centromere contacts in *Hs* vs. *Sc* plotted according to level of chromosome ploidy (aneuploid vs. euploid shown in Figure S3B). **(B)** 3D average representations of the *Sc* and *Hs* corresponding to complete chromosome-contact maps from Figure 2A. Color code highlight a few chromosomes with either short or long arms, as well as centromeres (CENs) and telomeres (TELs). **(C)** Schematic model of Rabl-like organizations of wild-type yeast chromosomes (*Sc* top panel) compared to the

histone-humanized (*Hs* bottom panel) one, showing de-clustering of centromeres. Examples of chromosome arms (gray lines) anchored at the nuclear membrane through CENs and TELs.

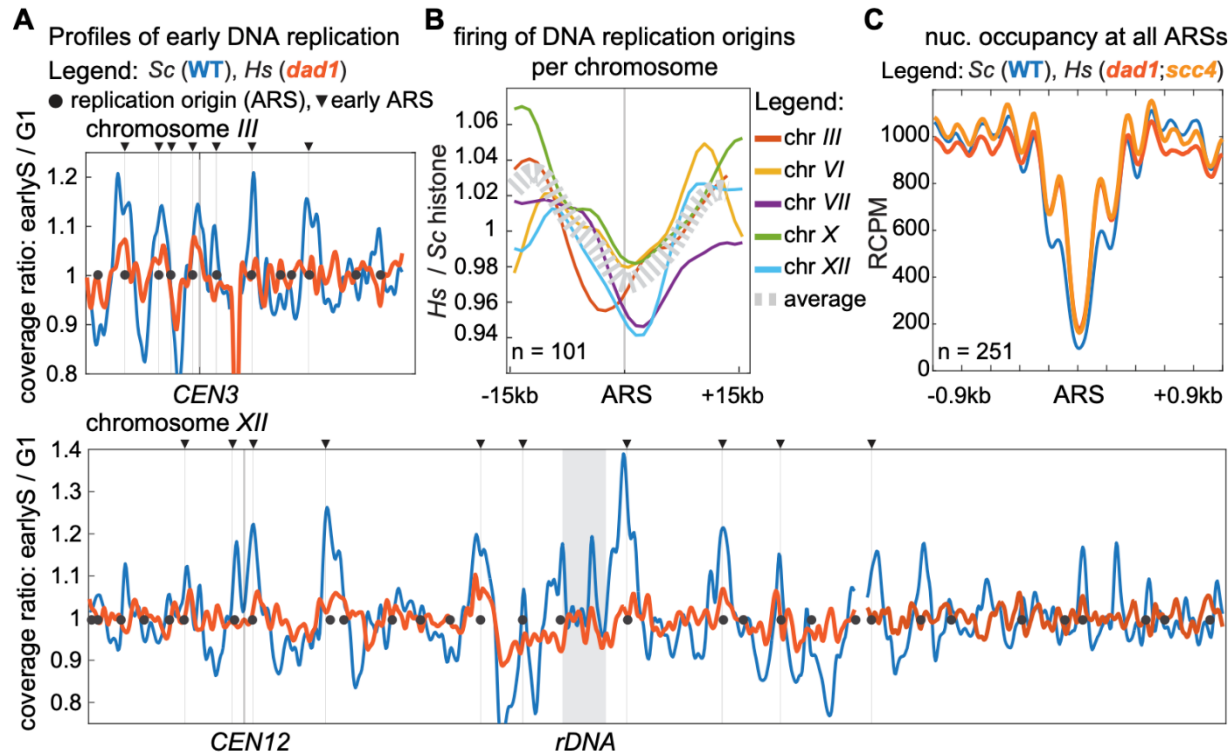


**Figure 4. Lack of temporal activation of replication origins on humanized chromosomes.**

**(A)** Each track in the replication timing plots is the average representation of three independent replicates and shows the sequencing coverage ratio of early-S (HU arrested) synchronized cells normalized to the G1 (a-factor arrested) non-replicating cells (1 kb-bin size) (see also Figure S4). Replication timing profiles of the wild-type (Sc) are shown in blue, while those of the histone-humanized strain (Hs, yDT180 *dad1*-E50D) are in orange. Representative profiles of chromosome III (top left) and chromosome XII (bottom left) are shown; positions of all origins (ARS) are indicated with black circles and arrowheads indicate the early ARS subset. **(B)** Metaplots of ARS activation were computed on chromosome-by-chromosome ratios between Hs and Sc profiles (see also Figure S5) and plotted in 30 kb ARS-centered windows. **(C)** Metaplots showing nucleosome occupancy from MNase-sequencing profiles at ARSs in Hs (yDT180 *dad1*-E50D and yDT92 *scc4*-D65Y) compared to Sc strains.

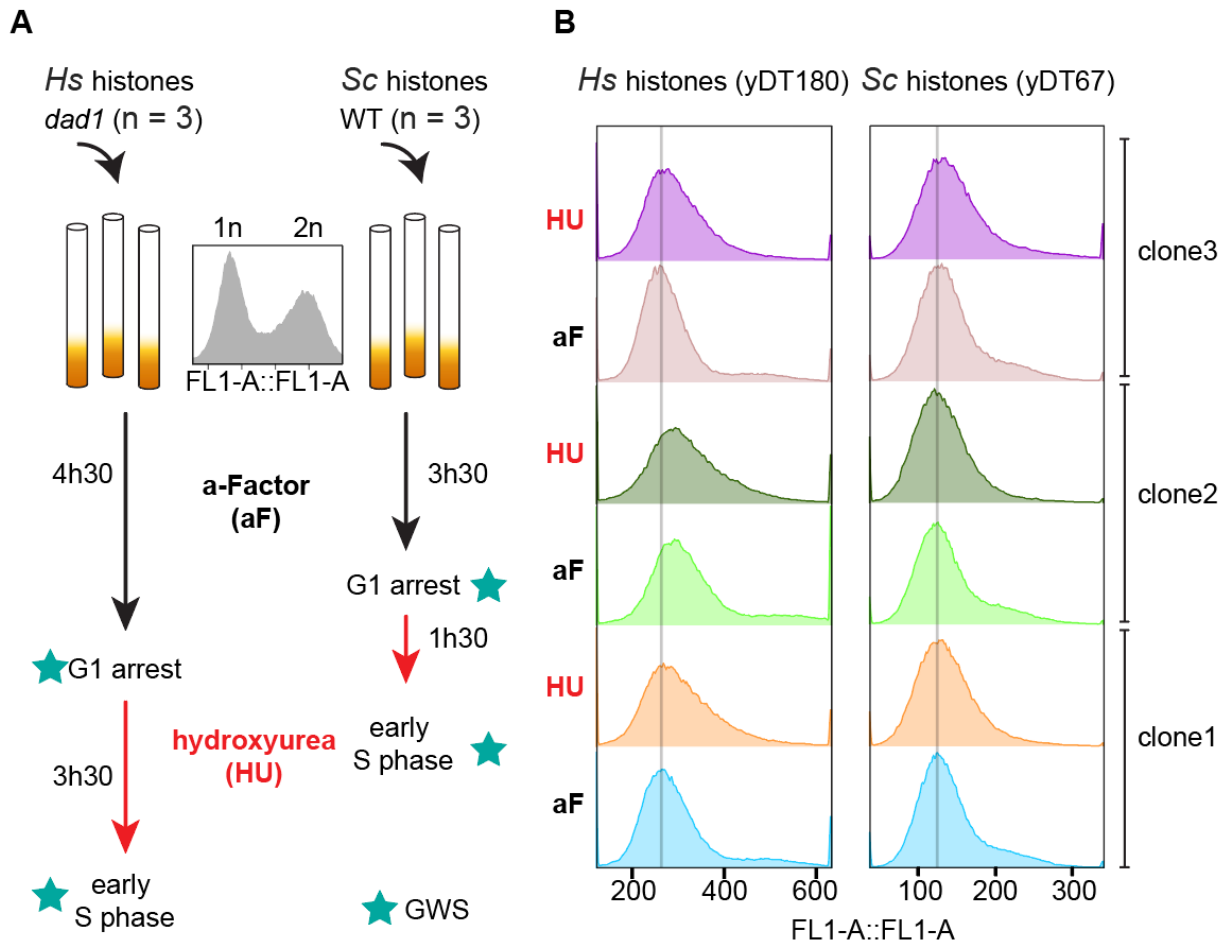


**Figure S4, related to Main Figure 4. Method for mapping replication timing in wild-type and histone-humanized yeasts.**

**(A)** Schematics of the experimental approach used to grow and synchronize yeast cells with either native (*Sc*) or human (*Hs*, strain: yDT180 *dad1*-E50D) histones in G1 and early S phase. Star-labeled steps indicate genome-wide sequenced samples used to generate replication timing profiles. **(B)** Flow cytometry histograms measuring DNA content of the three independently synchronized cell cultures in A, stained with SYTOX Green. As expected, no obvious differences are observed between G1 and early-S phase synchronized cells.

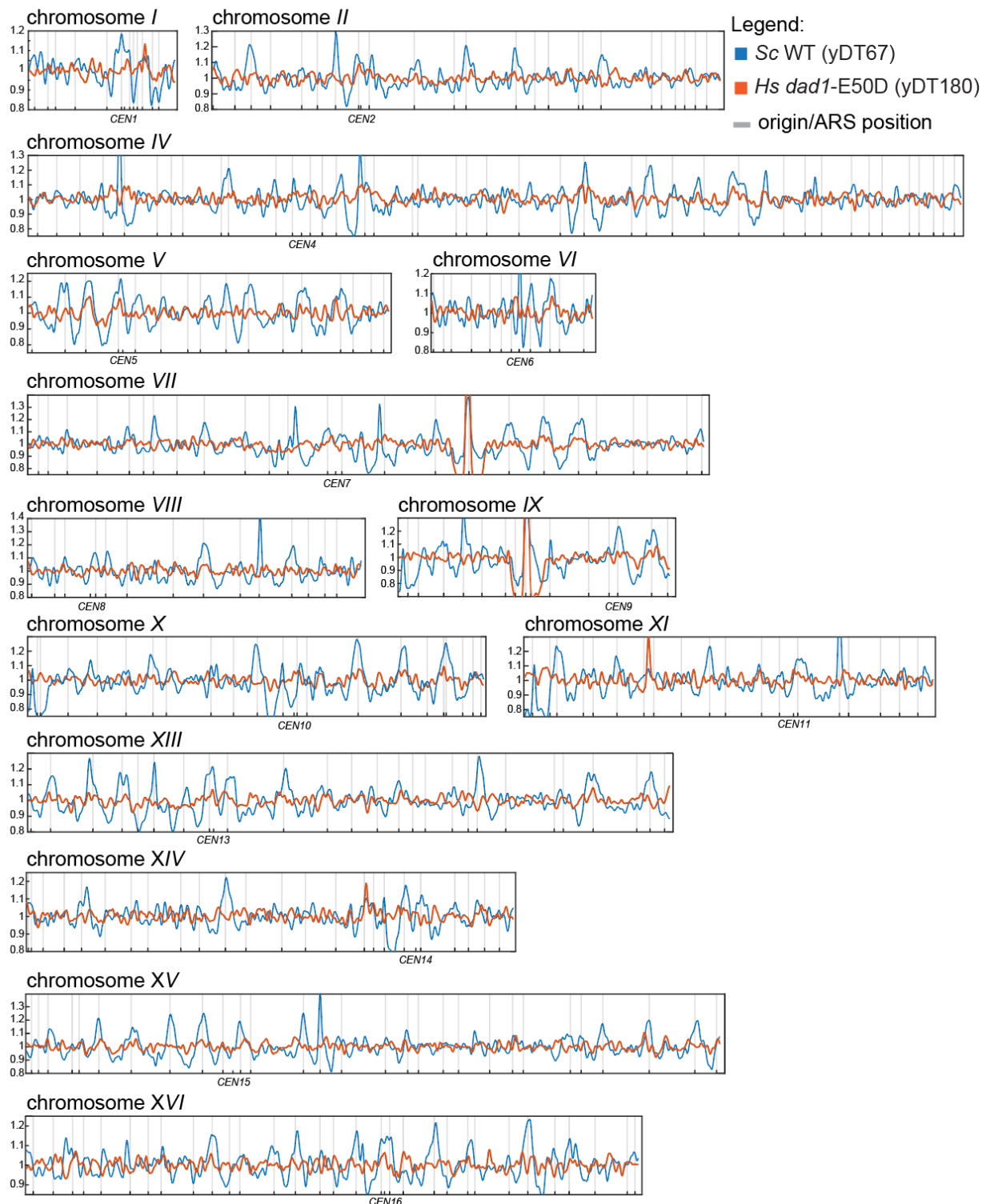


**Figure S5, related to Main Figure 4. Genome-wide replication timing profiles in wild-type and histone-humanized yeast strains.**

Each track in the replication timing plots is the average representation of three independent replicates and shows the sequencing coverage ratio of early-S (HU) synchronized cells

normalized on the G1 (a-factor) non-replicating cells (1 kb-bin size). Chromosome-by-chromosome replication timing profiles of the wild-type (*Sc*) are shown in blue, while those of histone-humanized (*Hs*, yDT180 *dad1-E50D*) are in orange. Origin (ARS) positions are indicated with gray vertical lines and centromere (CEN) positions are indicated below each plot.

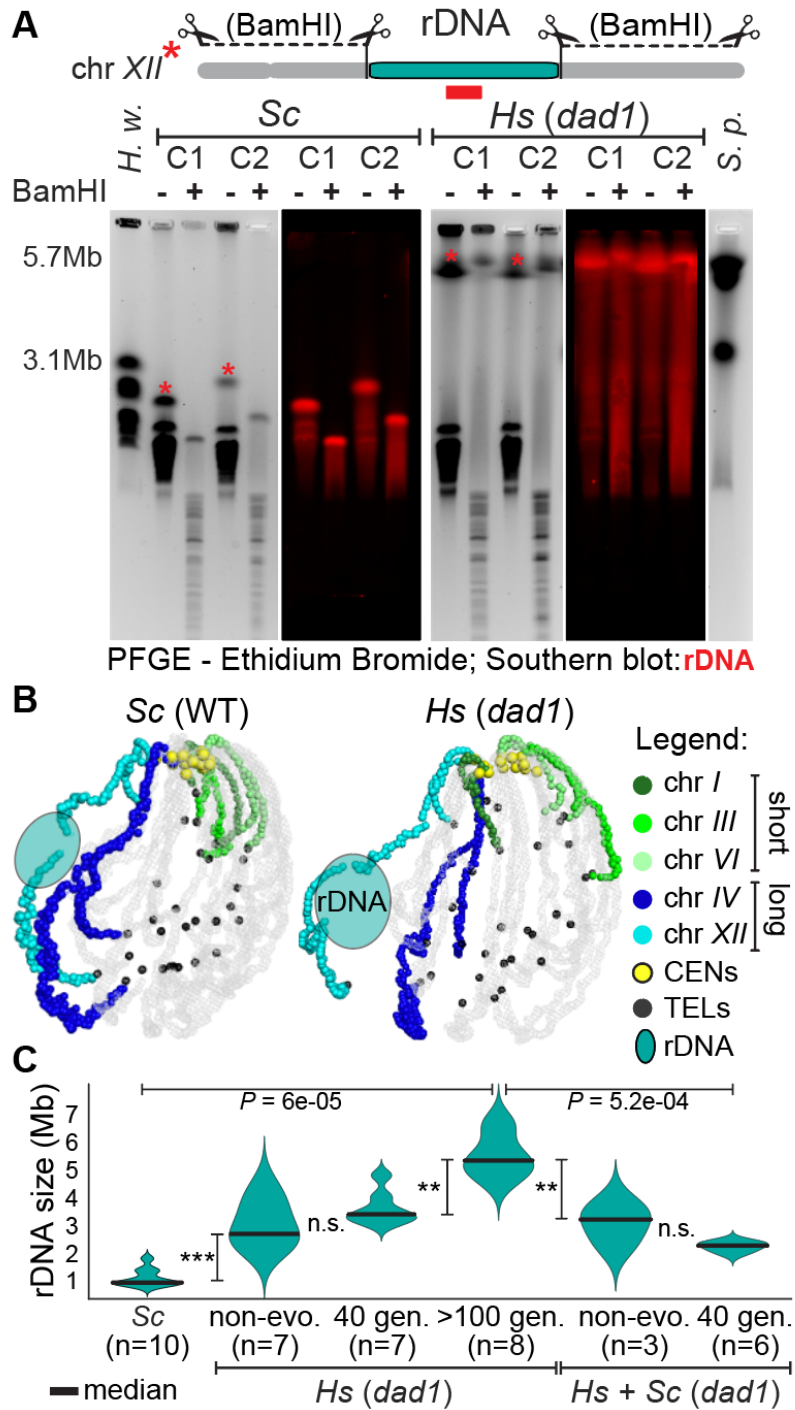


**Figure 5. Histone humanization leads to the intra-chromosomal expansion of the repeated rDNA array.**

**(A)** Estimate rDNA locus sizes (turquoise region on chromosome XII) in *Sc* and *Hs* (yDT180 *dad1*-E50D) strains. PFGE of yeast chromosomes digested (+) or not (-) with BamHI and the corresponding Southern blot with an rDNA specific probe (red). Each “C#” represents an

independent isolated clone of either *Sc* or *Hs* strain (see also [Figure S6A](#)). Left ladder: *H. wingei* chromosomes. Right ladder: *S. pombe* chromosomes. (\*) indicates chromosome XII. PFGE run specifications: *S. pombe* program for multi-megabase chromosome separation. **(B)** 3D average representations of the *Sc* and *Hs* Hi-C contact maps (as described in [Figure 3B](#)) where the estimated position of the rDNA locus is indicated (see also [Figure S6B](#)). Color code highlight a few short and long chromosomes, as well as centromeres (CENs) and telomeres (TELs). **(C)** Violin plots showing the estimated rDNA size (Mb) calculated using rDNA-mapped reads ( $n = \#$  genome sequencing datasets) in *Sc*, histone-humanized (*Hs*: “non-evo.” = non-evolved/passaged isolates; “40 gen.” and “>100 gen.” = passaged for # generations) and “re-yeastified” (native *Sc* histones added back to the humanized yeast) strains (see also [Figure S9F](#), [Table S2](#)).  $P$  values were calculated using the K–S (Kolmogorov–Smirnov) test.

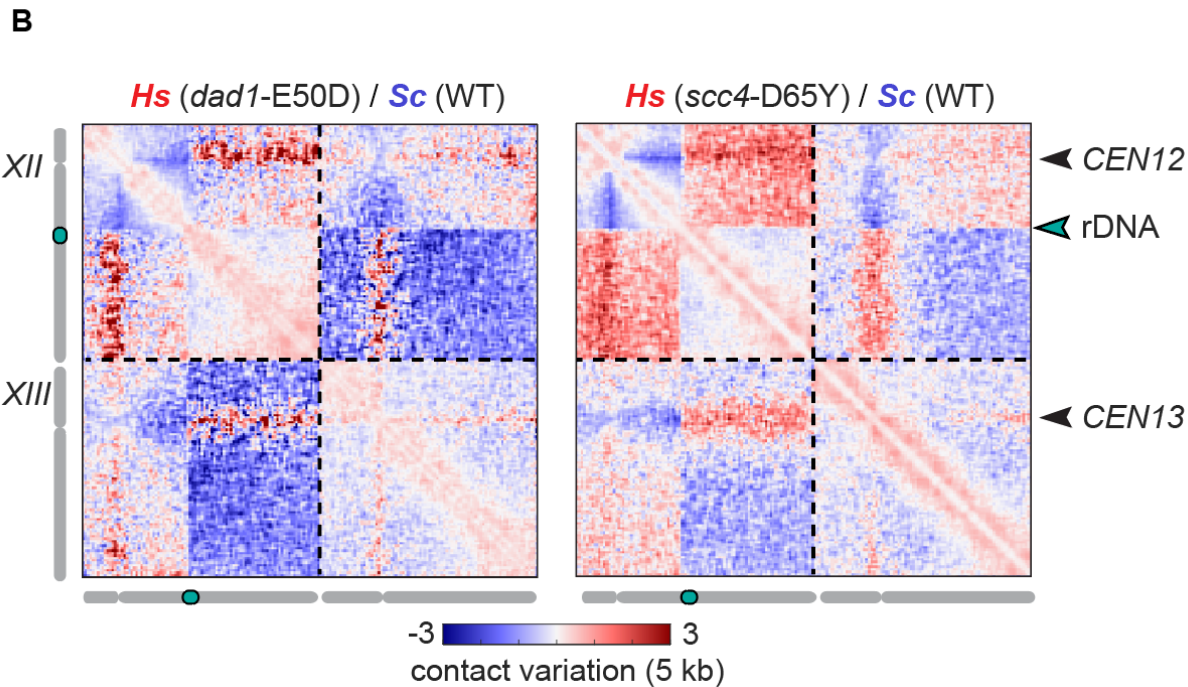
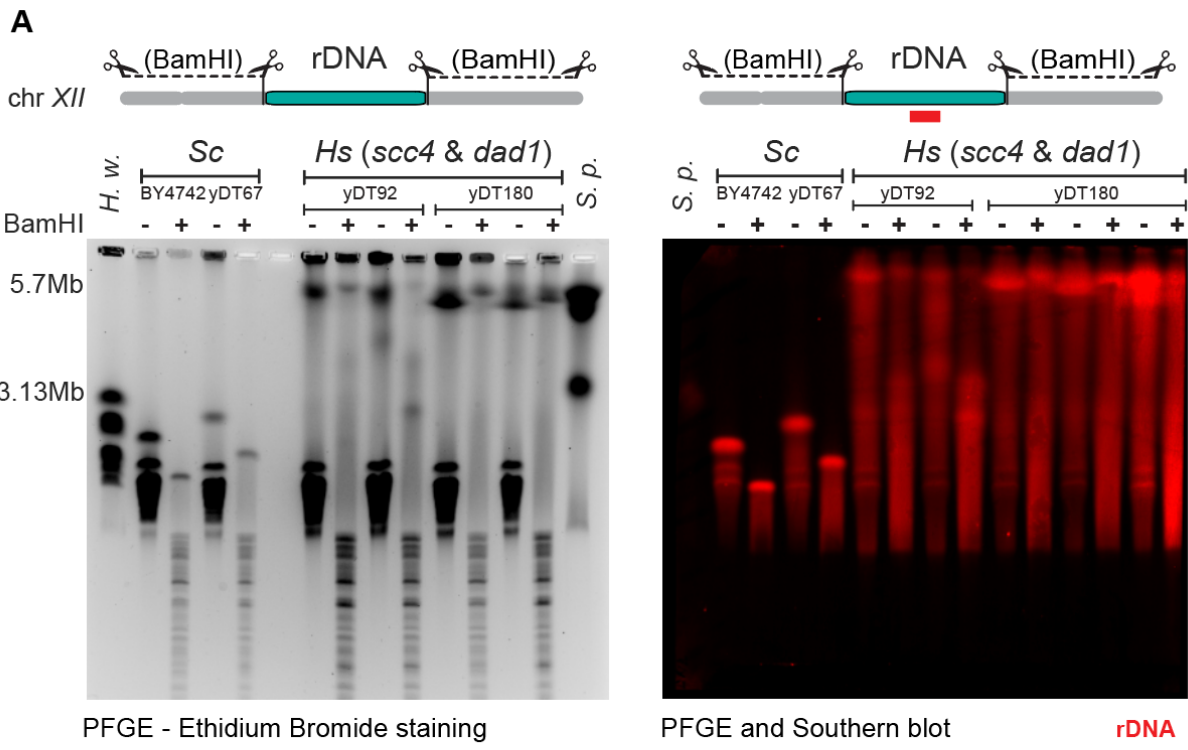


**Figure S6, related to Main Figure 5. Histone humanization leads to the expansion of the rDNA array.**

**(A)** Estimated rDNA locus sizes (turquoise region on chromosome XII) in independent isolates of *Sc* (strains: BY4741, yDT67) and *Hs* (strains: yDT92, yDT180) yeasts. PFGE of chromosomes digested (+) or not (-) with BamHI (left panel) and the corresponding Southern

blot (right panel) with an rDNA specific probe (red). PFGE ladders: *H. wingei* chromosomes (left) and *S. pombe* chromosomes (right). PFGE run specifications: *S. pombe* program for multi-megabase chromosome separation. **(B)** Contact map comparisons showing chromosomes *XII* and *XIII*. Log2-ratio maps of *Hs* vs. *Sc* strains: yDT180 *dad1*-E50D (left) and yDT92 *scc4*-D65Y (right). Arrowheads indicate the positions of the two centromeres and the rDNA locus. Color bar indicates contact variation between samples (log2 ratios 5 kb-binned).

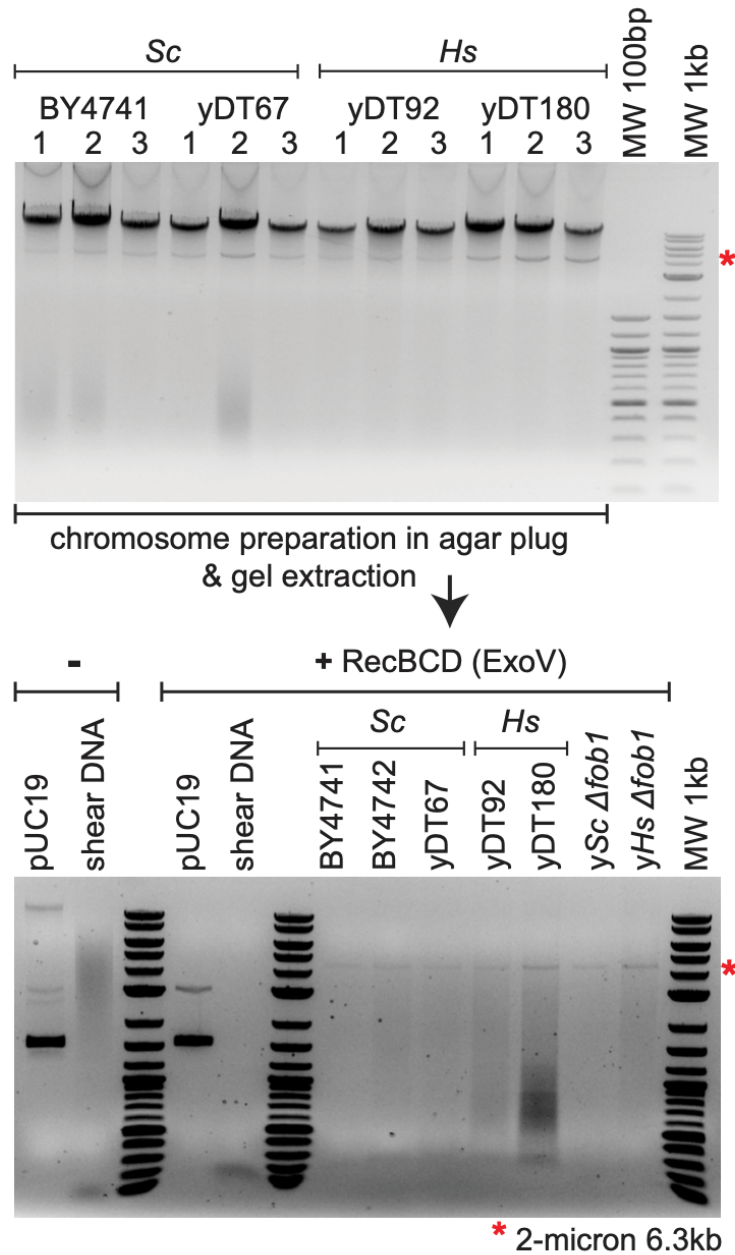


**Figure S7, related to Main Figure 5. Histone humanization does not lead to extra-chromosomal rDNA circles.**

Agarose gels stained with ethidium bromide showing: (top panel) total genomic DNA extracted from *Sc* (strains: BY4741, yDT67) and *Hs* (strains: yDT92, yDT180) yeasts and (bottom panel) after RecBCD treatment. pUC19 circular plasmid and sheared DNA were used as controls. Note that strains with the *FOB1* gene deleted were also tested and represent negative controls for extra-chromosomal rDNA circles (ERCs) formation. Red (\*) indicates 2-micron plasmid (~40-60 copies/cell Broach 1982).

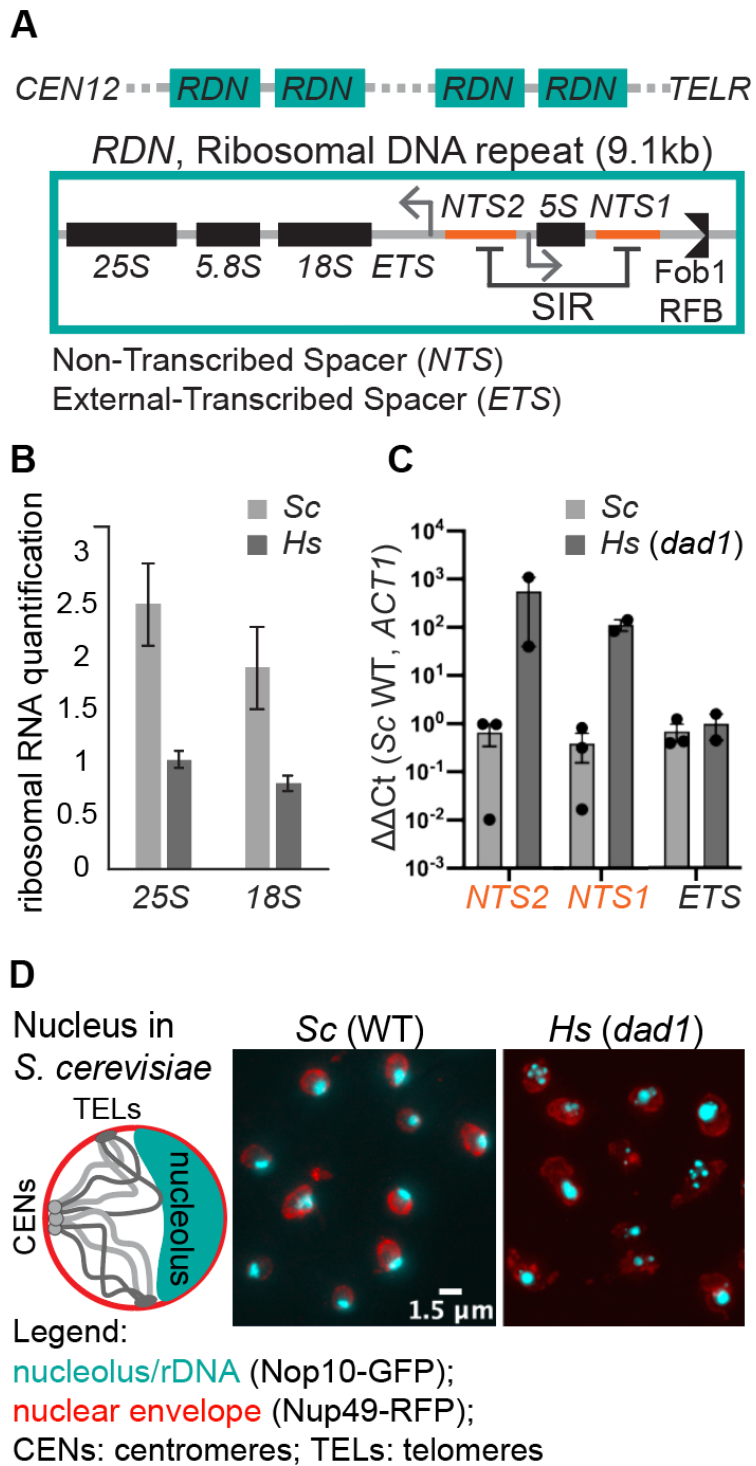


**Figure 6. Histone humanization disrupts rDNA silencing and nucleolar structure.**

**(A)** Schematic showing the organization of the *RDN1* array (rDNA locus on chromosome XII) and an inset on an example repeat (~9.1 kb-long), showing rRNA genes and regulatory sequences (*NTS1* and *NTS2* silenced by SIR complex, and Fob1 binding to the Replication

Fork Block, *RFB*). **(B)** Quantification of rRNA levels (18S and 25S) in triplicates of *Sc* and *Hs* (yDT180 *dad1*-E50D) strains. Total RNA was extracted from equivalent amounts of cells then quantified on agarose gel using ImageJ (see [Figure S9B](#)). **(C)** RT-qPCR bar plot used to estimate changes in the transcription of the *NTS1/2* and the rRNA precursor (*ETS*) relative to the housekeeping mRNA, *ACT1* (see [Figure S9C](#)). **(D)** Left, a simplified representation of nuclear organization in yeast, where examples of chromosome arms (gray lines) are anchored at the nuclear membrane through CENs and TELs, and the crescent-shaped nucleolus (turquoise) are shown. Right, representative microscopy images of *Sc* (strain: yLS110) or *Hs* (strain: yLS117) yeast nuclei. Nuclear envelope is shown in red (Nup49-RFP) and the nucleolus in cyan (Nop10-GFP).

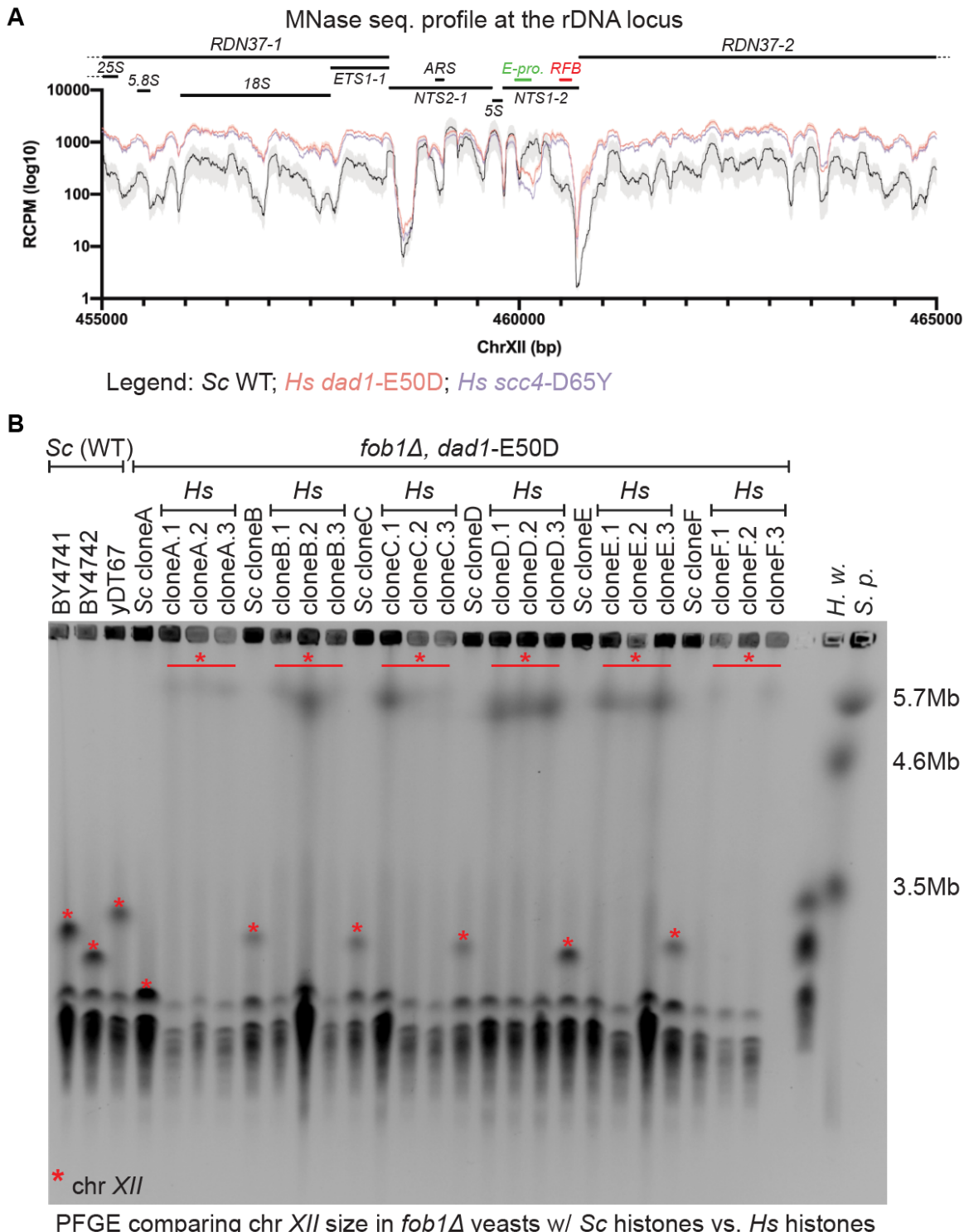


**Figure S8, related to Main Figure 6. rDNA instability is independent of the replication fork block.**

**(A)** MNase-sequencing coverage profiles at the rDNA locus in *Sc* and *Hs* strains (re-analyzed data from Truong and Boeke, 2017). **(B)** PFGE of yeast chromosomes in *fob1Δ* strains (Fob1,

rDNA replication fork block-binding protein). *FOB1* was deleted in *Sc* (clones A to F; strains yMAH1242-12447) followed by histone humanization *Hs* (clones: A# to F#; yLS118-123). Each lane represents an independent isolated clone. PFGE ladders on the right: *H. wingei* and *S. pombe* chromosomes. (\*) indicates chromosome XII. PFGE run specifications: *S. pombe* program for multi-megabase chromosome separation.

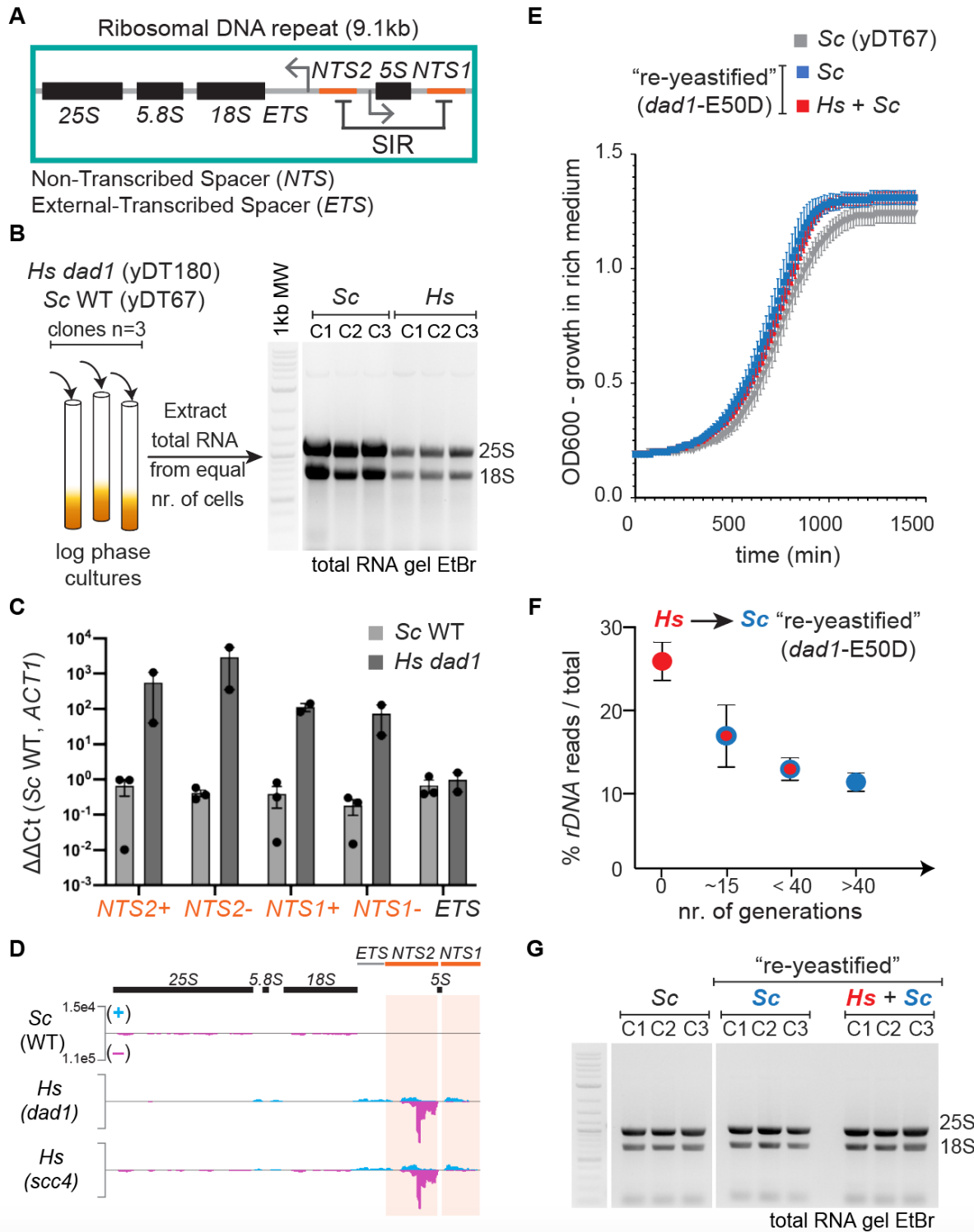


**Figure S9, related to Main Figure 6. The epigenetic instability of the rDNA depends on human histones and is reversible.**

**(A)** Schematic showing the organization of a ribosomal DNA repeat unit with rRNA genes (25S, 18S, 5.8S and 5S) and regulatory sequences (NTS1 and NTS2 silenced by SIR complex). **(B)**

Diagram of RNA extractions from triplicates of *Sc* (yDT67) and *Hs* (yDT180 *dad1*-E50D) strains and agarose gel used for rRNA quantifications in [Figure 6B](#). **(C)** RT-qPCR bar plot used to estimate changes in the transcription of the *NTS1/2* (“+” and “-“ DNA strands transcribed from the bidirectional E-promoter located in *NTS1*) and the rRNA precursor (*ETS*) relative to the control mRNA, *ACT1* (see [Table S3](#)). **(D)** Total RNA-sequencing coverage tracks at the rDNA unit in *Sc* and *Hs* strains (see [Table S4](#)). *y*-axis normalized to read counts per million. **(E)** Growth curves in rich media of the “re-yeastified” strains with *dad1*-E50D mutation (without *Hs* histones, *Sc*: yMAH753-755; *Hs* histones-maintained, *Hs* + *Sc*: yMAH756-758). **(F)** rDNA read count of the “re-yeastified” strains in [Figure 5C](#). **(G)** RNA gel of the “re-yeastified” strains, as described in panel E (*Sc*: yMAH753-755; *Hs* + *Sc*: yMAH756-758), relative to the wild-type *Sc* (yDT67) strain.